Chapter 4

Investigating the host-specificity of *Plasmodium* merozoite: primate erythrocyte interactions in the *Laverania* family

4.1 INTRODUCTION

4.1.1 The *Laverania* family of great ape parasites are host-specific.

P. falciparum is relatively divergent from the other species of *Plasmodium* that routinely infect humans; *P. vivax, P. malariae* and *P. ovale* (Liu *et al*., 2010; Prugnolle *et al*., 2011; Sharp *et al*., 2011). As outlined in the General Introduction (Chapter 1, Section 1.3), its closest relatives are found amongst a family of great ape parasites called *Laverania* which consists of six well-defined and closely related clades that appear to be strictly host-specific (Liu *et al*., 2010; Rayner *et al*., 2011). The clades *P. reichenowi* (C1), *P. gaboni* (C2) and *P. billcollinsi* (C3) have been found only in chimpanzees, whereas the *P. praefalciparum* (G1), *P. adleri* (G2) and *P. blacklocki* (G3) lineages appear to be restricted to gorillas. Within the *Laverania* family, *P. falciparum* is genetically most similar to *P. praefalciparum*; in fact *P. falciparum* mitochondrial DNA sequences form a single narrow group within the much broader spectrum of the *P. praefalciparum* sequences in phylogenetic trees. *P. falciparum* is therefore currently believed to have been derived from *P. praefalciparum* by means of a single cross-species transmission event from gorilla to human, dated to have occurred approximately 1 million-112,000 years ago (Liu *et al.,* 2010; Rayner *et al.,* 2011). The postulated gorilla-origin of *P. falciparum* and the continued presence of *P. falciparum*-like parasites in great apes pose two important questions with serious implications for global malaria eradication;

1. Are great apes a potential reservoir for *P. falciparum*?

2. Are the current *Laverania* strains harboured by great apes a possible source for future human infections?

Whether *P. falciparum* can successfully infect great ape species other than humans is a matter of debate. Although it has not yet been detected in wild living chimpanzees or gorillas, *P.*

falciparum has been identified in chimpanzees held in captivity close to human populations, suggesting that they are susceptible to anthroponosis of human-derived *P. falciparum* (Duval *et al.,* 2010). However, it has been shown that under experimental conditions even splenectomised chimpanzees show only low to moderate parasitemia when transfused with *P. falciparum* infected human blood and do not develop severe 'malignant tertian malaria' observed in human patients (Martin *et al.,* 2005). Conversely, from the evidence to date, *P. falciparum* appears to be the only *Laverania* species capable of infecting humans. Attempts to infect humans with *P. reichenowi* using parasitized chimpanzee blood in the 1920s-30s were unsuccessful (Blacklock & Adler, 1922; Martin *et al.,* 2005). Exactly which *Plasmodium* species were used in these experiments is unclear, as species distinctions were based on morphological analyses at the time, so it is possible that other chimpanzee *Laverania* parasites, in addition to *P. reichenowi,* were also used. There are, however, no recorded attempts of gorilla-derived material being used for experimental human infection and due to their ethically dubious nature, such studies can never be repeated. Systematic molecular-based approaches will, therefore, be required, in order to understand whether *Laverania* parasites are restricted to a specific host in the natural environment and identify what would enable them to cross species barriers and adapt to a new host (Duval & Ariey, 2012).

4.1.2 The molecular basis of the *Laverania* host-specificity is poorly understood.

The molecular mechanisms that impose host-specificity must act at the vector-host and/or parasite-host interface of the *Plasmodium* life cycle (Rayner *et al*., 2011). Chimpanzees and gorillas harbour different *Laverania* species even when occupying the same geographical location and as *Anopheles* mosquitoes are not known to discriminate between these great apes, the host specificity of the *Laverania* clades is likely to be due to incompatibility at the parasite-

host interface (Rayner *et al*., 2011). Mosquito preferences, however, cannot be ruled out and remains an important line of inquiry.

As the blood-stage of these parasites is crucial for maintaining a sustained infection within the primate host and for host-to-vector transmission (via the formation of gametocytes), the invasion of erythrocytes by the parasites has gained particular attention as a possible point of host-selection.

Of the numerous interactions between parasite and host cell surface proteins that mediate erythrocyte invasion, the EBA175-Glycophorin A interaction has been hypothesised to be one responsible for differences in host-selectivity between *Laverania* parasites (Chapter 3). *P. falciparum* EBA175 (*Pf*EBA175) and *P. reichenowi* EBA175 (*Pr*EBA175) have been observed to discriminate between human and chimpanzee erythrocytes when expressed as RII fragments on the surface of COS cells (Martin *et al*., 2005). This has been attributed to the difference in the sialic acid composition of human and chimpanzee erythrocytes due to the absence in expression of the CMAH gene in humans (Martin *et al*., 2005). The CMAH gene encodes an enzyme required for conversion of the Neu5Ac form of sialic acid to Neu5Gc, therefore human erythrocytes carry only Neu5Ac, whereas chimpanzee erythrocytes contain a mixture of the two, with Neu5Gc being predominant (Muchmore *et al.,* 1998). However, this sialic acid hypothesis does not explain the host-specificities of the *Laverania* family in general as chimpanzees and gorillas both carry active CMAH genes (Muchmore *et al.,* 1998).

4.1.3 The RH5-Basigin interaction as a possible determinant of host-specificity

The interaction of RH5 with its host receptor, Basigin (BSG), is essential for the invasion of human erythrocytes by *P. falciparum*, unlike the EBA175-Glycophorin A interaction which is only essential in some strains (Chapter 1, Section 1.7, Crosnier *et al.,* 2011). The contribution of

the RH5-BSG interaction towards determining host species-selectivity in the *Laverania* family has not been addressed before, but a previous study investigating the ability of different *P. falciparum* strains to invade erythrocytes of the new world monkey, *Aotus nancymaae*, suggested that polymorphisms in RH5 can influence the establishment/crossing of host-species barriers, in at least this instance (Hayton *et al.,* 2008). The hypothesis that the RH5-BSG interaction plays a similar role in the context of the *Laverania* family is therefore worth investigating.

4.1.4 Work described in this chapter

The molecular basis for the observed host-specificity within the *Laverania* family has previously not been investigated in a systematic manner. In this study, the potential contribution of two important parasite ligand-host receptor interactions, EBA175-Glycophorin A and RH5-BSG, towards the determination of host-specificity in *Laverania* was investigated. EBA175 RII orthologues from three *Laverania* species, namely the human parasite *P. falciparum* and two chimpanzee parasites *P. reichenowi* and *P. billcollinsi*, were expressed recombinantly and tested for specific binding to both human erythrocytes and purified native human Glycophorin A. RH5 orthologues from *P. falciparum* and *P. reichenowi* were also expressed and their interactions with human erythrocytes and recombinant BSG orthologues from three primates; human, chimpanzee (*Pan troglodytes*) and gorilla (*Gorilla gorilla*), were analysed. Site-directed mutants of human and chimpanzee BSG proteins were then generated and tested against *P. falciparum* RH5 to identify residues that confer species-selectivity.

4.2 RESULTS

4.2.1 EBA175 RII orthologues from three *Laverania* species were expressed and immunologically characterised.

The *P. falciparum* (3D7 strain) and *P. reichenowi* EBA175 sequences are publicly available (Ozwara *et al*., 2001; Gardner *et al*., 2002). The coding sequences of EBA175 orthologues from other *Laverania* species have now been derived by PCR-based sequencing of parasite genetic material, recovered from the fecal samples of wild-living chimpanzees in sub-Saharan Africa, by collaborators at the University of Pennsylvania, USA. The complete coding sequence for RII of the EBA175 ectodomain was obtained only for the chimpanzee parasite, *P. billcollinsi* (Weimin Liu and Beatrice Hahn, unpublished data). The EBA175 RII orthologues of *P. falciparum* (*Pf*EBA175 RII), *P. reichenowi* (*Pr*EBA175 RII) and *P. billcollinsi* (*Pb*EBA175 RII) exhibit a high degree of similarity (~ 80%) at the amino acid level (Figure 25).

In this study, these EBA175 RII orthologues were produced in soluble recombinant form to investigate their ability to interact with human erythrocytes and purified native human Glycophorin A. The coding sequences for *Pf*EBA175 RII and *Pr*EBA175 RII were PCR-amplified from expression constructs of their respective full-length ectodomains, *Pf*EBA175 FL (protein accession number: Q8IBE8) and *Pr*EBA175 FL (Q9N9G9) as described in section 2.1.1.1. The coding sequence for *Pb*EBA175 RII was assembled by gene synthesis for this study. The proteins were expressed in the human HEK293E cell line, with a mammalian signal peptide to ensure secretion into the culture medium.

The EBA175 RII orthologues produced with C-terminal Cd4 and biotin tags, were confirmed to be expressed at the expected size of ~ 97 kDa, by Western blotting (Figure 26 A). To determine whether they were correctly folded, their recognition by the two mouse monoclonals, R217 and

Figure 25. Sequence alignment of EBA175 RII orthologues from three species of *Laverania*. The amino acid sequences of RII of EBA175 from *P. falciparum* (*Pf*EBA175 RII), *P. reichenowi* (*Pr*EBA175 RII) and *P. billcollinsi* (*Pb*EBA175 RII) are shown. Conserved residues are shaded in black and semi-conserved residues in grey. The numbering indicated is for *Pf*EBA175 RII. The two DBL domains, F1 (aa 462-710) and F2 (aa 159-396) are marked in purple and green respectively. Sequences: *Pf*EBA175 RII (protein accession number Q8IBE8, aa 142-764), *Pr*EBA175 RII (Q9N9G9, aa 131-770). The *Pb*EBA175 RII sequence was obtained from Weimin Liu and Beatrice Hahn at the University of Washington, USA. The sequences were aligned using ClustalW software (Larkin *et al*., 2007).

R218, was tested by ELISA as performed before for *Pf*EBA175 FL (Section 3.2.1). R217 and R218, raised against a baculovirus-expressed *Pf*EBA175 RII antigen, have previously been characterised to bind non-linear, heat-labile epitopes within the F2 and F1 domains of RII respectively (Sim *et al.*, 2011). All three EBA175 RII orthologues were recognised by R218, but R217 only appeared to bind to *Pf*EBA175 RII and *Pr*EBA175 RII (Figure 26 B), suggesting that it recognises a region that is divergent in *Pb*EBA175 RII.

4.2.2 All three EBA175 RII orthologues showed specific binding to human erythrocytes.

The binding of EBA175 RII orthologues to human erythrocytes was analysed using the fluorescent bead-based flow cytometry approach developed for the functional characterisation of *Pf*EBA175 FL (Chapter 3, Section 3.2.2).

Multivalent arrays of EBA175 RII orthologues were generated by direct immobilisation of the biotinylated proteins on streptavidin-coated Nile red beads. The minimum amount of each protein necessary for complete saturation of a set number of beads was determined by ELISA, as described before (Section 3.2.2, Figure 27 A). The protein-coated beads were then presented to human erythrocytes, which were either untreated or pre-treated with one of three enzymes: trypsin, chymotrypsin or neuraminidase. Binding of the fluorescently-labelled protein arrays to the erythrocytes was analysed by flow cytometry. Cd4-coated beads were used as a negative control in the assay. Enzymatic treatment of erythrocytes was used as a means of probing the specificity of any observed association of EBA175 RII-coated beads with erythrocytes. The EBA175-Glycophorin A interaction is known to be sensitive to treatment with trypsin and neuraminidase, but not chymotrypsin (Camus and Hadley, 1985).
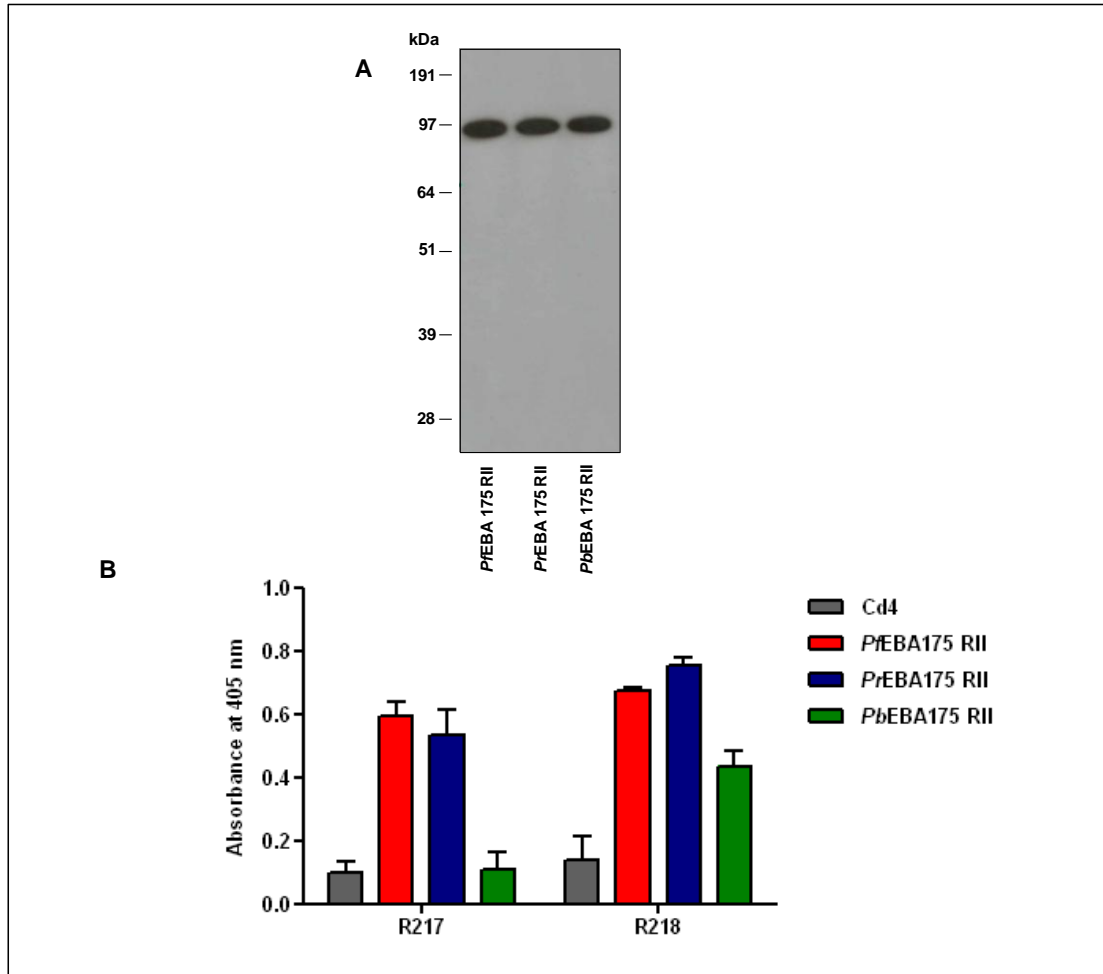
Figure 26. The EBA175 RII orthologues were expressed at the expected size of ~97 kDa and recognised by antibodies with conformation-specific epitopes. *Pf*EBA175 RII, *Pr*EBA175 RII and *Pb*EBA175 RII were expressed in the soluble form with C-terminal Cd4 and biotin tags using the HEK293E expression system. **A)** A Western blot of the EBA175 RII orthologues (~ 97 kDa) performed using HRP-conjugated extravidin as the probe. **B)** Recognition of the EBA175 RII orthologues by two mouse monoclonals, R217 and R218, which have been raised against a baculovirus-derived *Pf*EBA175 RII antigen and bind to non-linear epitopes. Binding of these monoclonals was detected by ELISA. Cd4 was used as the negative control in the assays. All ELISAs were performed on streptavidin-coated plates, using an alkaline phosphatase-conjugated anti-mouse antibody as the secondary. Alkaline phosphatase activity was quantified by the turnover of the colourimetric substrate, *p*-nitrophenyl phosphate, measured as an increase in absorbance at 405 nm. The graphically presented data indicate mean ± standard deviation; *n*=3.

A significant degree of self-association was observed with the EBA175 RII-coated beads and when evaluating the flow cytometry data, these aggregates were eliminated by gating on the erythrocyte population (Figure 27 B). The percentage of erythrocytes in each gated population that were binding to EBA175 RII-coated beads was calculated based on a fluorescence intensity threshold, set for selecting cells with a higher fluorescence at the Nile red emission wavelength than those incubated with Cd4-coated beads (Figure 28 A).

All three of the EBA175 orthologues showed clear and comparable binding to untreated and chymotrypsin-treated erythrocytes. Between 80-90% of erythrocytes in each of these populations were observed to interact with the EBA175 RII-coated beads (Figure 28 B and C). In comparison, only 1-4% of trypsin and neuraminidase-treated erythrocytes showed any binding to EBA175 RII-coated beads, suggesting almost no interaction of EBA175 RII orthologues with such cells.

4.2.3 Purified native human Glycophorin A was recognised by all three EBA175 RII orthologues in a sialic acid-dependent manner.

The binding of the EBA175 RII orthologues to commercially-available native Glycophorin A, (purified from human erythrocytes), was also directly compared using the ELISA-based approach developed for the characterisation of *Pf*EBA175 FL (Chapter 3, Section 3.2.3). An asialylated derivative of Glycophorin A was included in this assay as a negative control.

The Glycophorin A preparations were biotinylated *in vitro* (for immobilisation on streptavidin-coated plates) and quantified relative to each other by ELISA, prior to being tested against EBA175 RII (Figure 29 A). The EBA175 RII orthologues, expressed as β lactamase-tagged pentamers, were also normalised against each other by monitoring their enzymatic activity in a
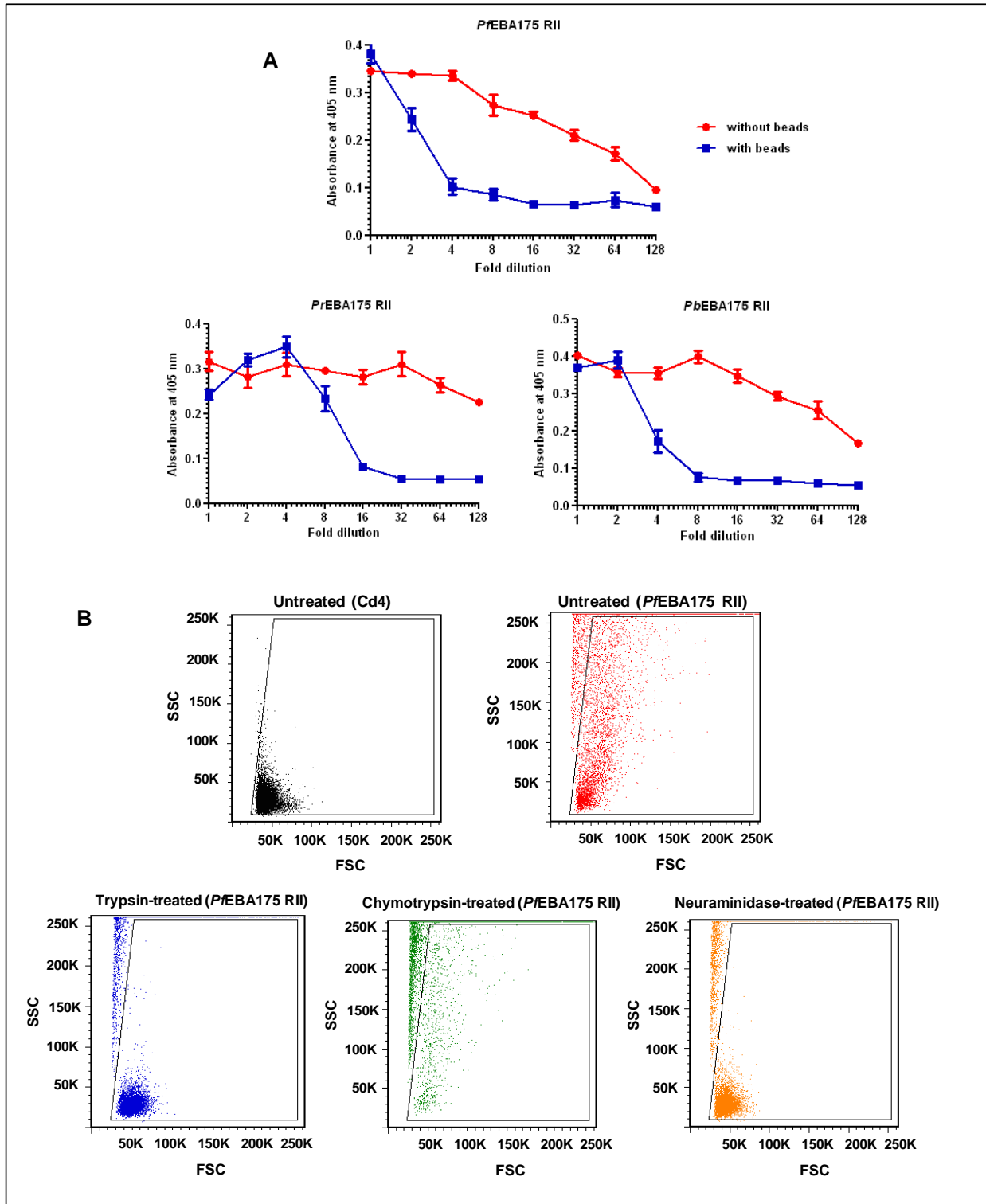
Figure 27. The EBA175 RII orthologues, multimerised on fluorescent beads, were presented to erythrocytes and analysed by flow cytometry. To monitor the binding of EBA175 RII orthologues to human erythrocytes, multimeric arrays of the proteins were generated by immobilising on streptavidin-coated Nile red beads. Erythrocytes were incubated with these arrays for 1 h at 4°C before analysis by flow cytometry. **A)** To determine the minimum amount of each EBA175 RII orthologue necessary for complete saturation of a set number of streptavidin-coated Nile red beads, ELISAs were performed on 2-fold serial dilutions of the proteins, with and without pre-incubation with beads. The ELISAs were carried out on a streptavidin-coated plate, using OX68 as the primary antibody and an alkaline phosphatase-conjugated anti-mouse antibody as the secondary. Data is shown as mean ± standard deviation; n=3. **B)** Dot-plots of the FSC (α size) and SSC (α granularity) parameters of the untreated and enzymatically-treated erythrocyte populations incubated with *Pf*EBA175 RII-coated beads, estimated by flow cytometry. Red: untreated erythrocytes. Erythrocytes pre-treated with trypsin, chymotrypsin and neuraminidase are shown in blue, green and orange respectively. The polygonal gate marked was used for separating the cells from bead aggregates. Erythrocytes incubated with Cd4-coated beads (negative control) are shown in black for comparison.
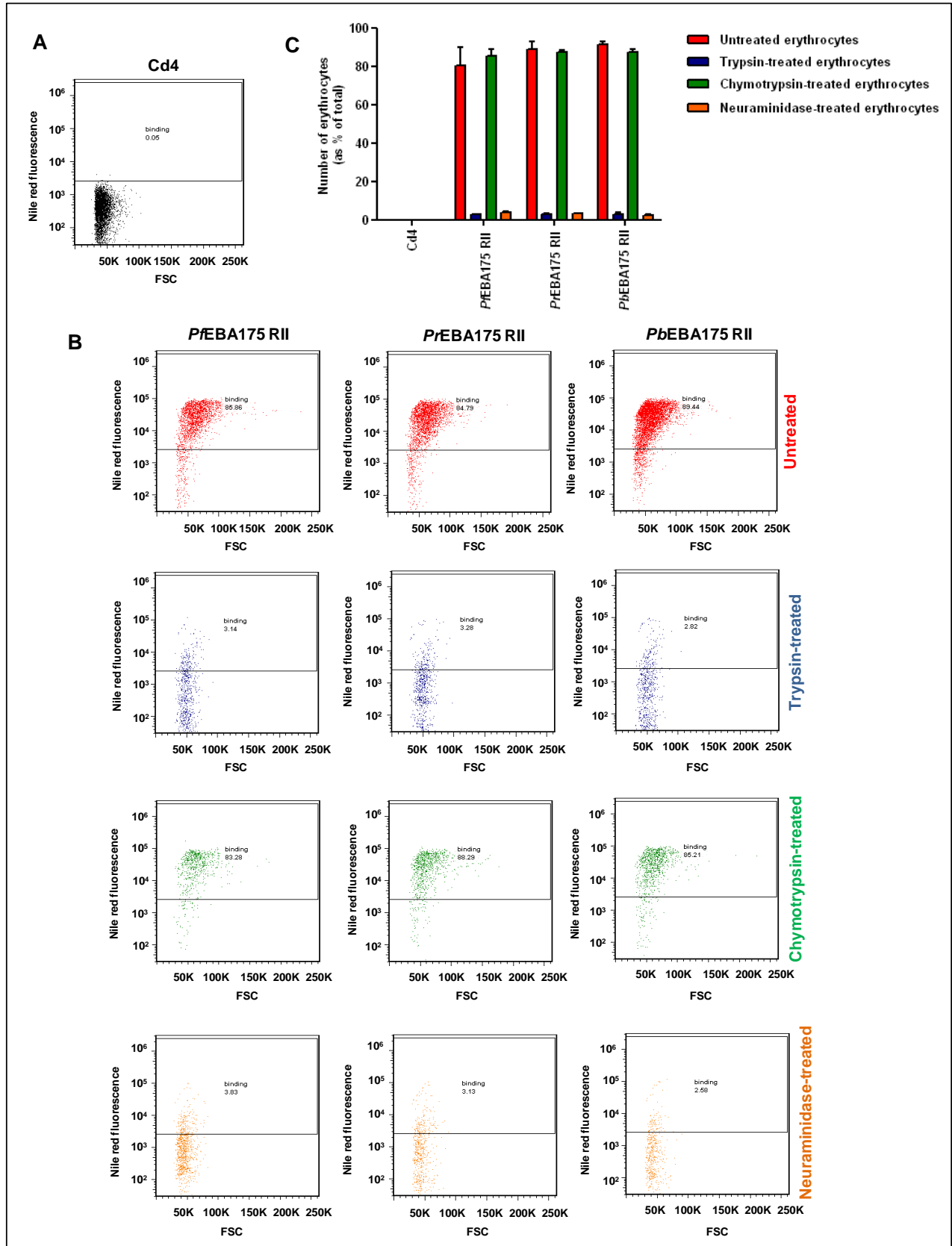
Figure 28. All three EBA175 RII orthologues showed significantly more binding to untreated and chymotrypsin-treated erythrocytes, than to trypsin and neuraminidase-treated cells. A and **B** show dot plots of Nile red fluorescence intensity *versus* FSC for erythrocyte populations incubated either with Cd4-coated beads (**A**) or with EBA175RII-coated beads (**B**). The rectangular gate marked was used to estimate the fraction of Nile red 'positive' cells. The range of fluorescence intensities exhibited by cells incubated with Cd4-coated beads (the negative control) was used to determine the lower threshold of this gate. **C** is a bar chart representing the numbers of erythrocytes (as a percentage of total) binding to EBA175 RII-coated beads. In **B** and **C**, untreated cells are shown in red. Erythrocytes pre-treated with the enzymes trypsin, chymotrypsin and neuraminidase are indicated in blue, green and orange respectively.

time course assay (Figure 29 B).

All three of the EBA175 RII orthologues showed significantly more binding to sialylated Glycophorin A than to its asialylated derivative (Figure 29 C). The variation in the binding responses of the EBA175 RII orthologues with Glycophorin A could be indicative of the differential affinities of the interactions. However, this could also be due to discrepancies in the amount of functional EBA175 between the samples. Filtered culture supernatants containing EBA175 were used in this assay, rather than purified proteins and although care was taken to normalise the amount of recombinant protein in the supernatants by monitoring the activity of the β-lactamase fusion tag, this was only an approximate measure.

4.2.4 SPR studies revealed differences in the affinities of the EBA175 RII orthologues for human Glycophorin A.

In order to conclude whether the EBA175 RII orthologues bind human Glycophorin A with different affinities, it was therefore necessary to perform further analysis with SPR using purified EBA175. The K_D for the *Pf*EBA175 RII-Glycophorin A interaction was previously estimated to be ~2.5 µM (Chapter 3, section 3.2.9).

For this study, the three EBA175 RII orthologues, expressed with C-terminal Cd4 and hexa-His tags, were purified from the culture supernatant by affinity chromatography on nickel-charged Sepharose. The final yield of each purified protein was approximately 0.1 mg/100 ml culture. Analysis of the proteins by denaturing SDS-PAGE confirmed their expression at the expected size of ~97 kDa (Figure 30 A). When subjected to gel filtration prior to SPR analysis, each protein was observed to elute as a single peak at ~34 ml (corresponding to a molecular weight of ~70 kDa), indicating a monomeric form (Figure 30 B).
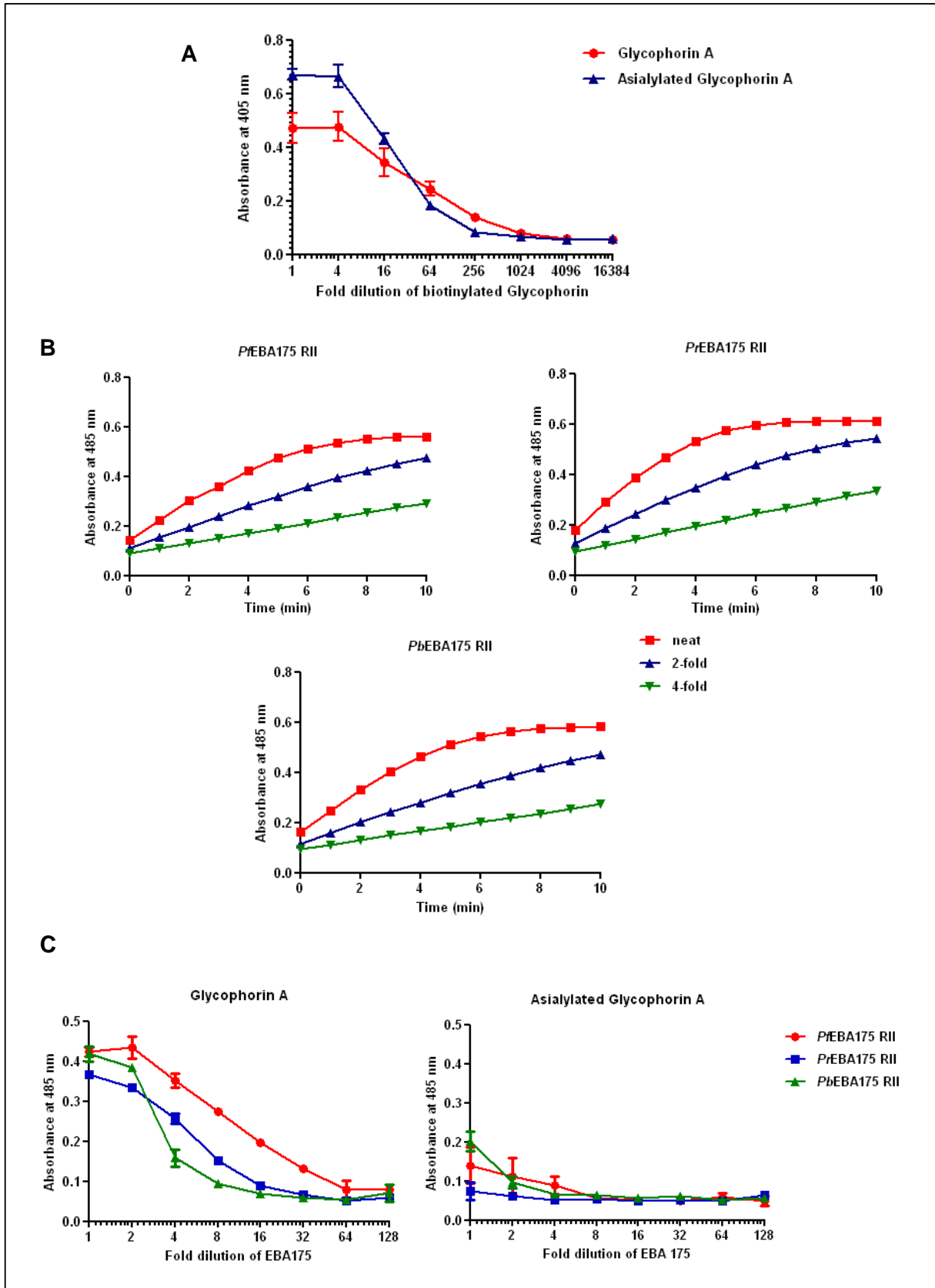
Figure 29. An ELISA-based assay was used to compare the binding of the EBA175 RII orthologues to sialylated and asialyalted forms of native human Glycophorin A. The EBA175 RII orthologues, expressed as soluble β-lactamase tagged pentamers, were tested against two biotinylated Glycophorin A preparations, sialylated native Glycophorin A extracted from human erythrocytes and an asialylated derivative, immobilised on streptavidin-coated plates. **A)** The amount of biotinylated protein in each of the Glycophorin A preparations was normalised against each other by ELISA on a streptavidin-coated plate using BRIC256 (an anti-Glycophorin A mouse monoclonal) as the primary antibody and an alkaline phosphatase-conjugated anti-mouse secondary. The data are shown as mean ± standard deviation; $n=3$. **B)** The EBA175 RII orthologues expressed in the pentameric form with a β-lactamase tag, were normalised against each other using a time-course assay, monitoring the turnover of the colorimetric β-lactamase substrate, nitrocefin, at an absorbance of 485 nm. **C)** A 2-fold dilution series of each EBA175 RII orthologue was probed against Glycophorin A and binding was detected using nitrocefin. The pentameric proteins were incubated with the immobilised Glycophorin A for 2 h at room temperature and the absorbance at 485 nm was measured after overnight incubation with nitrocefin at 4°C. The data are shown as mean ± standard deviation; $n=3$.

The three EBA175 RII orthologues were first injected across biotinylated Glycophorin A, immobilised on a streptavidin-coated sensor chip, at equimolar concentrations, in succession. The binding responses of *Pr*EBA175 RII and *Pb*EBA175 RII were similar to each other but markedly lower than that of *Pf*EBA175 RII (Figure 30 C). To obtain estimates for the affinities of their interactions with Glycophorin A, a 2-fold serial dilution each of *Pr*EBA175 RII and *Pb*EBA175 RII were injected across the SPR sensor surfaces. The reference-subtracted sensorgrams were globally fitted to a steady-state 1:1 binding model. The predicted K_D values were similar, (5.0 ± 0.1) x 10^{-6} M and (5.3 ± 0.08) x 10^{-6} M respectively for the *Pr*EBA175 RII-Glycophorin A and *Pb*EBA175 RII-Glycophorin A interactions.

The observed shape of the reference-subtracted sensorgrams was typical of a two-stage reaction, with both association and dissociation of the soluble analyte, consisting of a fast phase, followed by a slower phase. Whilst this could be indicative of an interaction involving a conformational change of the proteins, it could also be due to the presence of aggregates in the analyte samples. When the EBA175 orthologues were gel filtered before the SPR analysis no multimeric forms were detected; however, aggregates could have formed after this stage.

The reference-subtracted sensorgrams could not be fitted to a 1:1 binding kinetic model with confidence. The K_D values calculated by local fitting of the curves to a two-state reaction model (Figure 30 D) were consistent with the estimates from the equilibrium analysis and suggested only a ~2-fold difference in the affinity for human Glycophorin A between *Pr*/*Pb*EBA175 RII and *Pf*EBA175 RII.
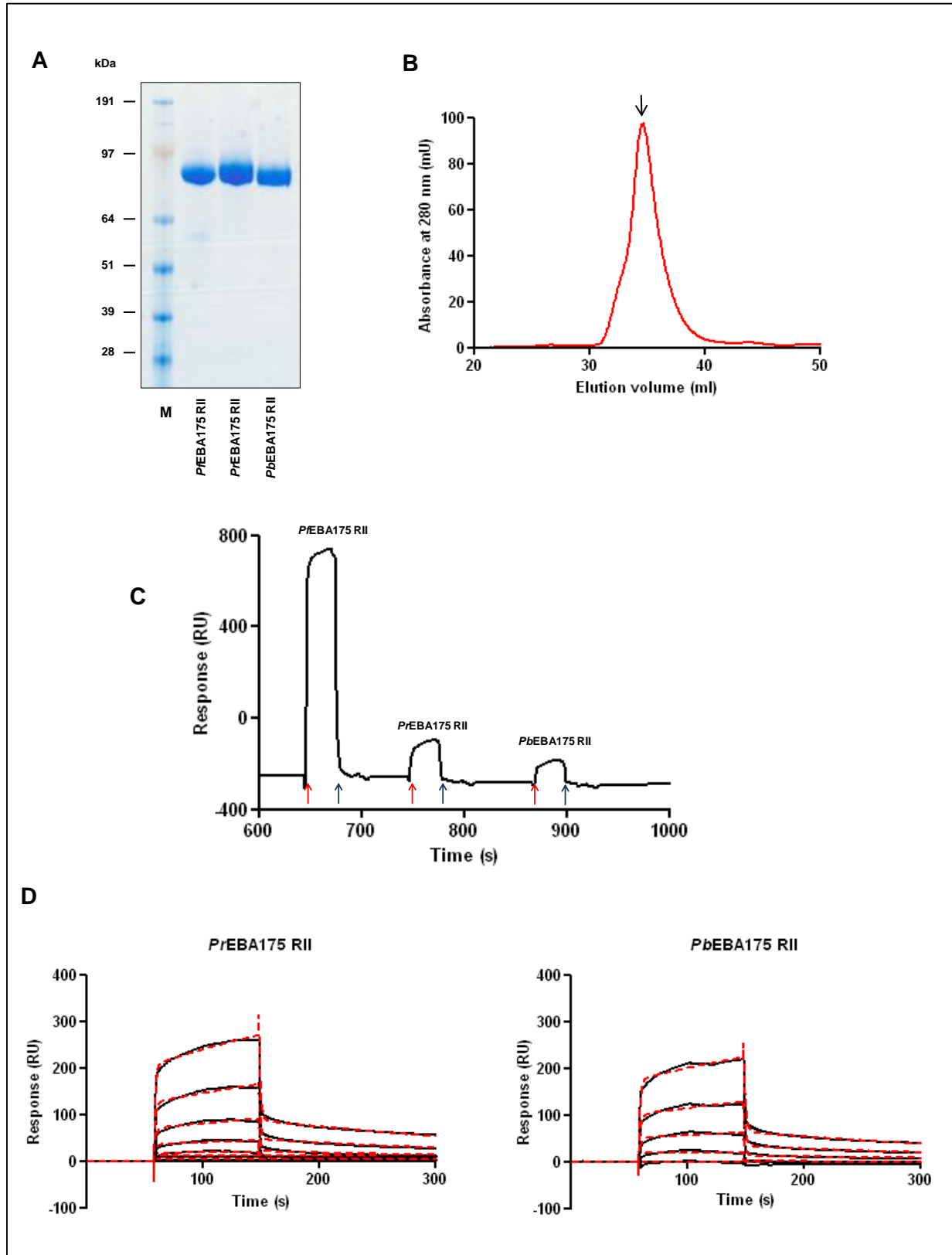
Figure 30. Hexa-His tagged EBA175 RII orthologues were purified from culture supernatants and tested against native Glycophorin A by SPR, to derive quantitative affinity estimates. A) Denaturing SDS-PAGE analysis of affinity-purified EBA175 RII orthologues. The proteins were visualised using Coomassie brilliant blue. **B**) The typical elution profile of an EBA175 RII orthologue from gel filtration. The peak fraction at ~34 ml is indicated by ▼ . **C**) Reference subtracted sensorgram from the sequential injection of the three EBA175 RII orthologues, each at 3 μM, over biotinylated native Glycophorin A immobilised on a streptavidin-coated sensor chip. The red and blue arrows indicate the start and the end of each injection. The EBA175 proteins were injected at a flow rate of 10 μl/min for 30 s each. **D**) Reference subtracted sensorgrams from the injection of a 2-fold dilution series (0.2-3.0 μM) each of *Pr*EBA175 RII and *Pb*EBA175 RII over immobilised Glycophorin A. The EBA175 proteins were injected at a flow rate of 20 μl/min, with a contact time of 120 s and a dissociation time of 200 s. The black lines represent experimental data and the red dotted lines, the local fitting to a two-state reaction model. The biotinylated baits were immobilised at Cd4 (reference)- 820 RU and Glycophorin A-980 RU.

4.2.5 RH5 orthologues from two *Laverania* species were expressed and biochemically characterised.

Whereas the EBA 175 orthologues of the *Laverania* parasites are relatively highly conserved, only approximately 68% sequence similarity is observed between the RH5 orthologues of *P. falciparum* (*Pf*RH5) and *P. reichenowi* (*Pr*RH5) (Figure 31), implying more scope for species-specific recognition.

In this study, *Pf*RH5 and *Pr*RH5 were expressed in soluble recombinant form in order to compare their ability to recognise human erythrocytes and recombinant BSG. The predicted full-length coding sequences of both proteins were codon optimised for expression in the HEK293E system and their endogenous signal peptides (residues 1-24) were replaced by a mammalian-derived sequence. The potential N-linked glycosylation sites on both proteins were also removed during gene synthesis to prevent the inappropriate addition of carbohydrate moieties in the human secretory pathway. *Pf*RH5 and *Pr*RH5, produced with C-terminal Cd4 and biotin tags, were expected to be approximately 88 kDa in size. Analysis of these proteins by Western blotting confirmed their expression in the full-length form (Figure 32 A). A certain proportion of both proteins, however, appeared to be N-terminally processed, generating fragments of ~68 kDa and ~28 kDa (Figure 32 A). The processing of both *Pf*RH5 and *Pr*RH5 in a similar manner, suggests conservation of these proteolytic cleavage sites. The size of the Cd4 tag is ~25 kDa, therefore the ~88 kDa and ~68 kDa forms correspond well to the 63 kDa and 45 kDa native forms of *Pf*RH5 that have been observed in parasite cultures (Baum *et al*., 2009).

After normalisation by ELISA (Figure 32 B), the RH5 orthologues were tested against a panel of 27 mouse monoclonal antibodies that had been raised against a partially-glycosylated

```
                    25                                                        77
PfRH5    FENAIKKTKNQENNLALLPIKSTEEEKDDIK-------NGKDIKKEIDNDKENIKTNNAK
PrRH5    FENAKKKTKNQENNLALLPIKSSEEEKSNIKHKDIGNVNKDDINNDIDNDKKDVKISNVK
conservation   **** ****************** **** **.......* ** .***** .* * **

                    78                                                       136
PfRH5    DHSTYIKSYLNTNVNDGLKYLFIPSHNSFIKKYSVFNQINDGMLLNEKNDVKNN-EDYKN
PrRH5    DHSTYIKSYLNKNVNDGLKYLFMPSHNAYIKKYSLFNKMNNDMLLNEKKDVNNNKEDDKN
conservation   *********** ********** **** .***** ** .* ****** ** .** **

                    137                                                      196
PfRH5    VDYKNVNFLQYHFKELSNYNIANSIDILQEKEGHLDFVIIPHYTFLDYYKHLSYNSIYHK
PrRH5    INHKNVNFLQNDFKGLPKNNIADSIDIVQDKEGHLDFIIIPYYSHVEYCKHLSIISVFHR
conservation   .  ******* ** * *** ****.* ******* *** *. ..* **** *..*.

                    197                                                      256
PfRH5    SSTYGKCIAVDAFIKKINEAYDKVKSKCNDIKNDLIATIKKLEHPYDINNKNDDSYRYDI
PrRH5    LSTYGEYKDVIAFVKNINEKYDKVKDKCNEIKNDLITTIKKLENPHDVNNKNEDSNIYNT
conservation    ****    * **.* *** ***** *** *.****** * *.****.** *

                    257                                                      315
PfRH5    SEEIDDKSEE-TDDETEEVEDSIQDTDSNHAPSNKKKNDLMNRAFKKMMDEYNTKKKKLI
PrRH5    FEDIDDIYEDDMQDQLEYVYDTIEDADSDNTHPNKKKYHLINRAYKKMMDEYNLKKNKLI
conservation   *.***  *.. * * * *** * ** **** * .*** .******** ** ***

                    316                                                      375
PfRH5    KCIKNHENDFNKICMDMKNYGTNLFEQLSCYNNNFCNTNGIRYHYDEYIHKLILSVKSKN
PrRH5    QCIKNNEPDFNNIYMDIKNYATNRFENIACDNINFCNTNGIKNHYIYYIEKEMLAIKSKD
conservation    **** * *** * ** *** ** **.. * * ******* ** ** * .* ***

                    376                                                      435
PfRH5    LNKDLSDMTNILQQSELLLTNLNKKMGSYIYIDTIKFIHKEMKHIFNRIEYHTKIINDKT
PrRH5    LNKDIKDMTSILQQSELLLTNLNKKMGSYIYIDTIKFIHKEMKYIFKRIEHHTNIIIDKI
conservation   ****. *** ********* ************************ ** *** ** ** **

                    436                                                      495
PfRH5    KIIQDKIKLNIWRTEQKDELLKRILDMSNEYSLFITSDHLRQMLYNTFYSKEKHLNNIFH
PrRH5    KIIDDKYKISINKAFPKNILLPKILDLSNEYALFITSSTLRQMLYNTFYTKEKHLHNLFH
conservation   *** ** *. * * * ** .***.**** ***** ********** ***** *.**

                    496                              526
PfRH5    HLIYVLQMKFNDVPIKMEYFQTYKKNKPLTQ
PrRH5    HLIYVLQIKFNDVPVHMEYFPIYKKKKILTQ
conservation   *******. ******.. **** *** * ***
```

Figure 31. Sequence alignment of RH5 orthologues from *P. falciparum* and *P. reichenowi*. The amino acid sequences of RH5 from *P. falciparum* (*Pf*RH5) and *P. reichenowi* (*Pr*RH5) are shown. Conserved residues are shaded in black and semi-conserved residues in grey. The numbering indicated is for *Pf*RH5. Sequences: *Pf*RH5 (protein accession number Q8IFM5, aa 25-526), *Pr*EBA175 RII (B4X6H6, aa 25-535). The endoegnous signal peptides (aa 1-24) of *Pf*RH5 and *Pr*Rh5 were replaced by a mammalian leader sequence, prior to expression in HEK293E cells. The sequences were aligned using ClustalW software (Larkin *et al.*, 2007).

mammalian-expressed *Pf*RH5 antigen, by collaborators at the University of Oxford (Sandy Douglas, unpublished data). All the monoclonal antibodies, with the exception of 3AG12, were observed to bind to *Pf*RH5. *Pr*RH5 was however not recognised by any of the monoclonals (Figure 32 C). The absence of binding of 3AG12 to *Pf*RH5 might be due to recognition of a glycosylated epitope by this antibody.

Untreated and heat-treated samples of *Pf*RH5 and *Pr*RH5 were then tested against polyclonal sera raised against *Pf*RH5 in rabbit. Prior to this analysis, antibodies binding to the Cd4 tag were removed from the sera by pre-adsorption on immobilised Cd4. The binding of the polyclonal to *Pf*RH5 was reduced upon heat-denaturation of the former, suggesting the recognition of heat-labile epitopes in the antigen (Figure 32 D). In comparison to the negative control, Cd4, some slight binding of the polyclonal to *Pr*RH5 was observed. Heat-treatment of *Pr*RH5 appeared to have little effect on this binding, indicating recognition of one or more linear epitopes (Figure 32 D).

4.2.6 Both RH5 orthologues showed sialic acid-independent binding to human erythrocytes.

Multivalent arrays of *Pf*RH5 and *Pr*RH5, generated by direct immobilisation of the biotinylated proteins on streptavidin-coated Nile red beads, as described before for the EBA175 RII orthologues, were presented to untreated and neuraminidase-treated human erythrocytes, to observe any putative interactions. *Pf*EBA175 RII and Cd4-coated beads were included as the positive and negative controls respectively (section 4.2.2 above). Compared to the negative control, only about 5-8% of the erythrocytes were observed to associate with the RH5-coated beads (Figure 33 A and B). Neuraminidase-treatment of erythrocytes had almost no effect on this binding, as expected given that recognition of BSG by *Pf*RH5 is not known to be sialic acid dependent.
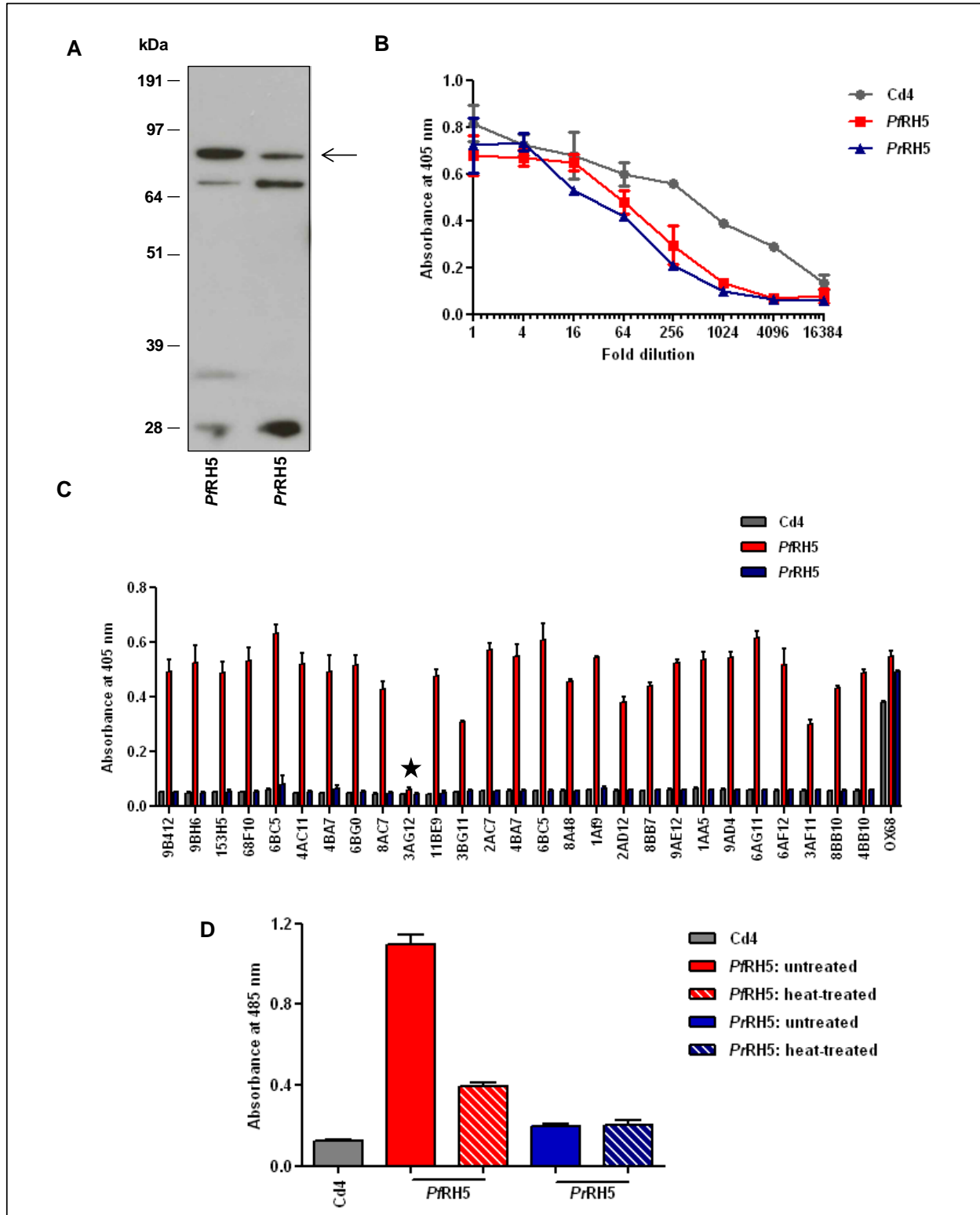
Chapter 4

Figure 32. The RH5 orthologues of *P. falciparum* and *P. reichenowi* were recombinantly expressed. *Pf*RH5 and *Pr*RH5 were expressed in the soluble form with C-terminal Cd4 and biotin tags using the HEK293E expression system. **A)** A Western blot of *Pf*RH5 and *Pr*RH5 performed using HRP-conjugated extravidin as the probe. The full-length form of each of the fusion proteins (88 kDa) is indicated with the arrowhead. **B)** Relative quantitation of *Pf*RH5 and *Pr*RH5, against Cd4 by ELISA. The anti-Cd4 mouse monoclonal OX68, was used as the primary antibody. **C)** Recognition of *Pf*RH5 and *Pr*Rh5 by a panel of 26 mouse monoclonal antibodies that had been raised against a partially-glycosylated mammalian-derived *Pf*RH5. ★– No binding of *Pf*RH5 was observed to 3AG12. OX68 was used as a positive control. **D)** Binding of untreated and heat-treated samples of *Pf*RH5 and *Pr*Rh5 to a polyclonal raised against *Pf*RH5. Prior to the assay, anti-Cd4 antibodies were removed from the sera by pre-adsorption on immobilised Cd4. Binding of the anti-RH5 antibodies was also detected by ELISA. Cd4 was used as the negative control in the assays. All ELISAs were performed on streptavidin-coated plates, using an alkaline phosphatase-conjugated anti-mouse antibody as the secondary. The graphically presented data indicate mean ± standard deviation; *n*=3.

The difference in the binding of *Pf*EBA175 RII and *Pf*RH5 to human erythrocytes was hypothesised to reflect the availability of their respective receptors, Glycophorin A and BSG, at the cell surface. This was tested by comparing the staining of erythrocytes by the anti-Glycophorin A monoclonal, BRIC256, with that by two anti-BSG mouse monoclonals, MEM-M6/1 and MEM-M6/2. The binding of these monoclonals were detected with the same FITC-conjugated anti-mouse secondary. The erythrocytes incubated with BRIC256 were observed to have a 10^2-fold higher median fluorescence intensity than those incubated with MEM-M6/1 and MEM-M6/6 (Figure 33 C and D), confirming much higher levels of expression of Glycophorin A on the erythrocyte surface, in comparison to BSG.

4.2.7 BSG orthologues from three species of primates were expressed and characterised.

Although both *Pf*RH5 and *Pr*RH5 showed some binding to human erythrocytes in the previous assay, whether they were recognising the same receptor on the erythrocyte surface could not be concluded. Therefore, to investigate whether *Pr*RH5 binds BSG (the known erythrocytic receptor of *Pf*RH5) and whether *Pf*RH5 and *Pr*RH5 show a preference for BSG from their natural host-species, full-length ectodomains of the BSG orthologues from human (*Homo sapiens*), chimpanzee (*Pan troglodytes*) and gorilla (*Gorilla gorilla*) were expressed in soluble recombinant form and tested against the two RH5 orthologues directly.

The short splice isoform of Basigin (BSG) is thought to be the major variant of this protein present on human erythrocytes. It comprises two IgSF domains in the extracellular region and has been shown to interact directly with *Pf*RH5 (Crosnier *et al*., 2011). The sequences for three predicted isoforms of Basigin in *P. troglodytes* and two in *G. gorilla* were retrieved from the
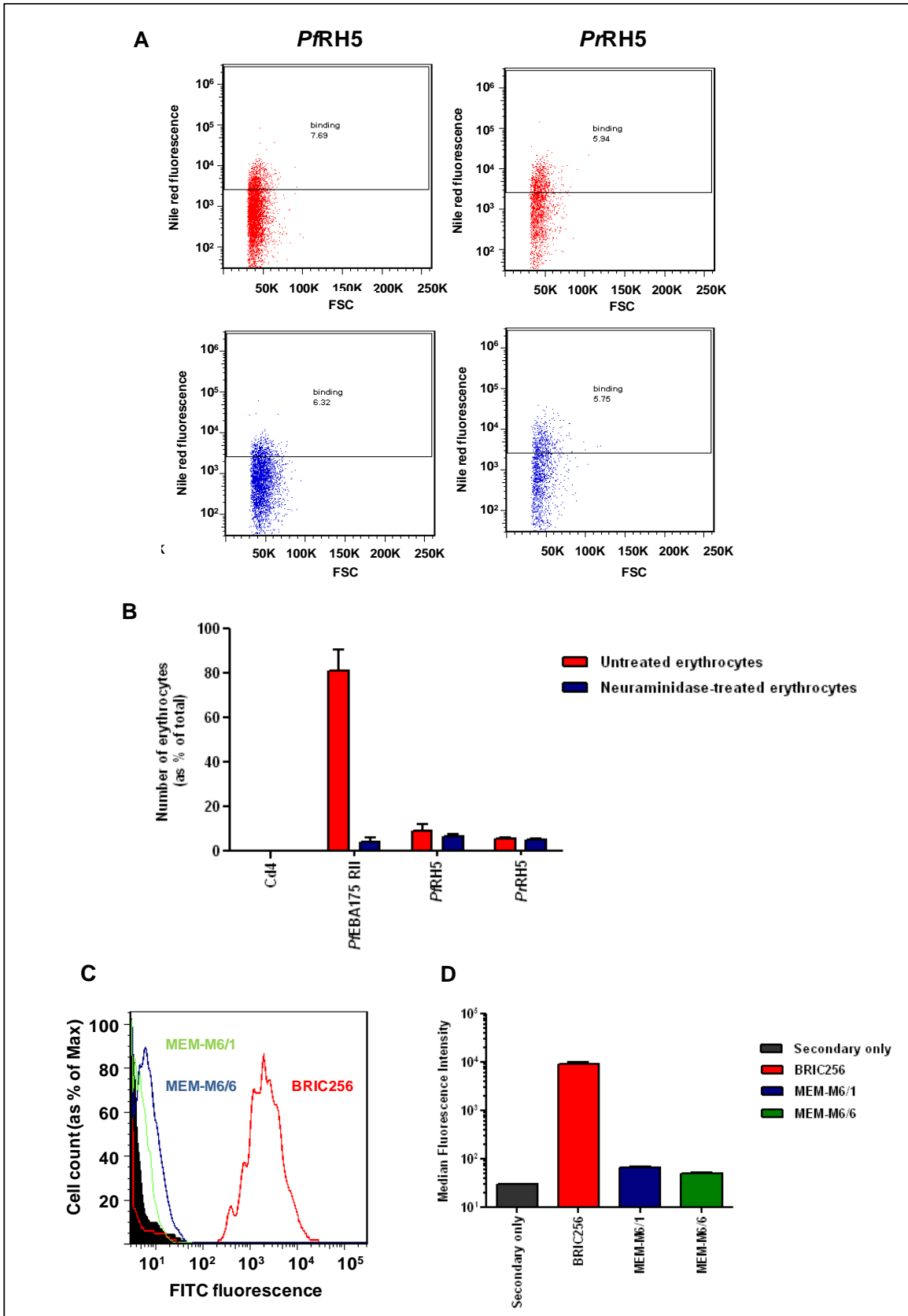
.

Figure 33. Both *P. falciparum* and *P. reichenowi* RH5 orthologues were observed to bind to human erythrocytes. Multimeric arrays of *Pf*RH5 and *Pr*Rh5, generated by immobilising the biotinylated proteins on streptavidin-coated Nile red beads, were incubated with untreated and neuraminidase-treated erythrocytes for 1 h at 4°C before analysis by flow cytometry. **A)** Dot plots of Nile red fluorescence intensity *versus* FSC for erythrocyte populations incubated with RH5-coated beads. The rectangular gate marked was used to estimate the fraction of Nile red 'positive' cells. The lower threshold of this gate was determined from the range of fluorescence intensities exhibited by erythrocytes incubated with Cd4-coated beads (the negative control) as previously (Figure 28 A). **B)** A bar chart representing the numbers of erythrocytes (as a percentage of total) binding to RH5-coated beads. The binding to beads coated with Cd4 (negative control) and *Pf*EBA175 RII (positive control) are also included for comparison. In **A** and **B**, untreated and neuraminidase pre-treated erythrocytes are shown in red and blue respectively. **C)** A histogram showing the staining of human erythrocytes by the mouse monoclonals BRIC256 (anti-Glycophorin A), MEM-M6/1 (anti-BSG) and MEM-M6/6 (anti-BSG), detected using a FITC-conjugated anti-mouse secondary. **D)** A bar chart of the median fluorescence intensity of the erythrocyte populations stained with BRIC256, MEM-M6/1 and MEM-M6/6 at the FITC emission wavelength. In **C** and **D**, the staining with BRIC256, MEM-M6/1 and MEM-M6/6 are shown in red, blue and green respectively. Erythrocytes incubated with only the secondary antibody (negative control) are represented in black. The bar charts show mean ± standard deviation; $n=3$.

Ensembl genome browser (Flicek *et al*., 2011). The InterPro Scan server (Zdobnov and Apweiler, 2001) was then used to analyse the possible domain architecture of these proteins. Only the isoforms with two IgSF domains, *P. troglodytes* ENSPTRP00000017252 (*Pt*BSG) and the *G. gorilla* ENSGGOP00000022655 (*Gg*BSG) were selected for expression (Figure 34 A). When the sequences of the selected BSG orthologues were aligned, the leucine at position 174 of human BSG (*Hs*BSG) was observed to be deleted in *Pt*BSG, but present in *Gg*BSG (Figure 34 B). This leucine residue, located on a linker region between two β strands (Yu *et al*., 2008) was found to be conserved in predicted BSG orthologues from other primates, including the great apes bonobo and orang-utan, rhesus macaque (an old world monkey) and common marmoset (a new world monkey), by performing a blast search with the *Hs*BSG sequence. Inspection of the *Pt*BSG transcript sequence and its annotations on the Ensembl browser, revealed that the deletion of Leu-174 was probably an error arising from incorrect specification of intron-exon boundaries. Therefore, when assembling the *Pt*BSG coding sequence by gene synthesis, a codon for leucine was introduced at the corresponding position. Overall, the *Hs*BSG, *Pt*BSG and *Gg*BSG orthologues were observed to share a notably high degree (~95%) of primary sequence similarity (Figure 34 B).

The BSG orthologues, expressed with C-terminal Cd4 and biotin tags, were first analysed by Western blotting to confirm their expression at the correct size. An un-glycosylated monomer of recombinant BSG was expected to have a molecular weight of ~44 kDa. All three BSG orthologues were observed as smears on the Western blot ranging in size between ~51 kDa and ~64 kDa (Figure 35 A). Each of these proteins carry three putative N-linked glycosylation sites, hence the smearing is likely due to the presence of different glycoforms.
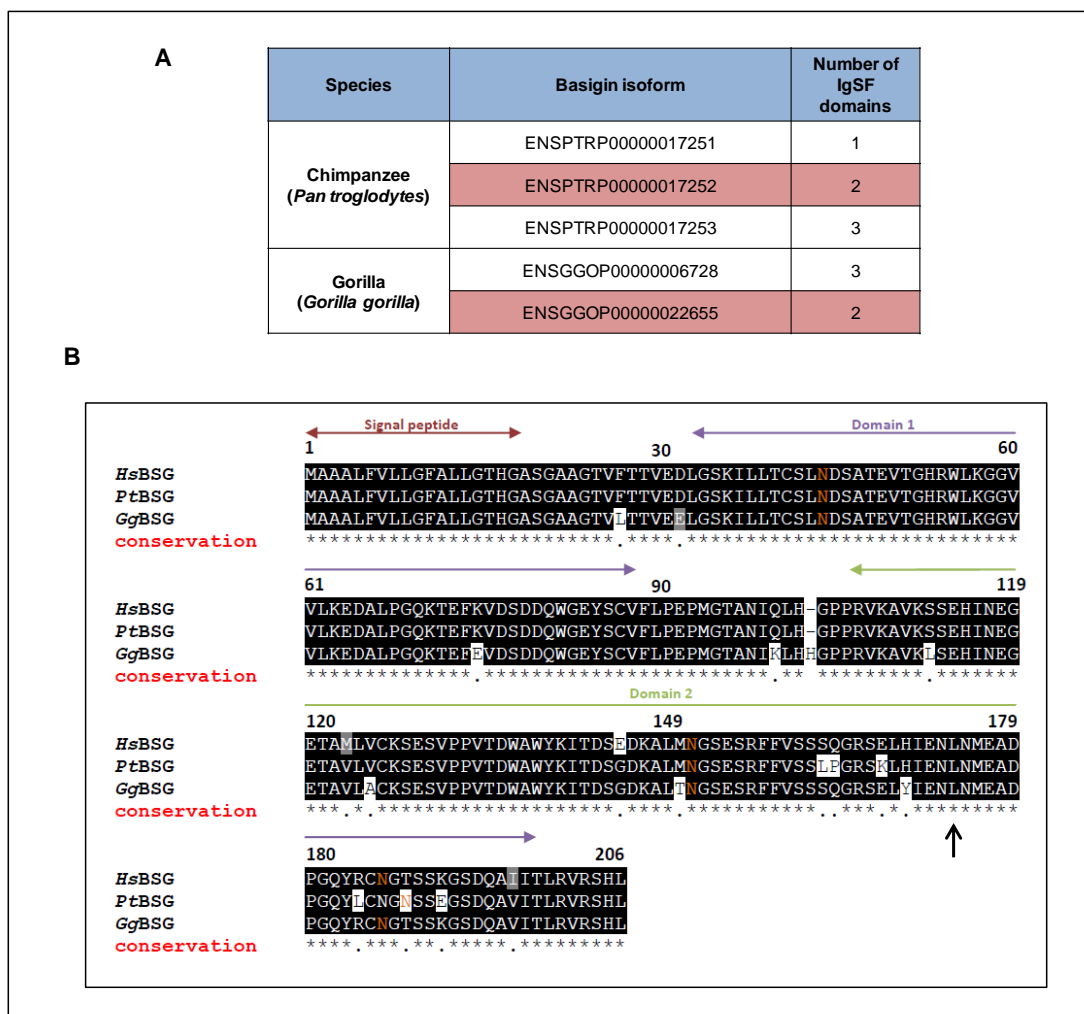
Figure 34. Basigin orthologues from human (*H. sapiens*), chimpanzee (*P. troglodytes*) and gorilla (*G. gorilla*): domain predictions and sequence alignments. A) The sequences of the predicted Basigin isoforms of *P. troglodytes* and *G. gorilla*, retrieved from the Ensembl genome browser (Flicek *et al*., 2011), were analysed for IgSF domains using InterPro Scan (Zdobnov and Apweiler, 2001). **B)** Alignment of the full-length ectodomains of BSG orthologues containing two IgSF domains from human (*Hs*BSG, protein accession number: NP_940991, aa 1-206), chimpanzee (*Pt*BSG, aa 1-206) and gorilla (*Gg*BSG, aa 1-207). Conserved residues are shaded in black and semi-conserved residues in grey. The numbering indicated is for *Hs*BSG. The signal peptide (aa 1-18), IgSF domain 1 (aa 20-88) and IgSF domain 2 (aa 100-204) are marked in maroon, purple and green respectively. The N-linked glycosylation sites on the proteins are shown in orange. The black arrow marks Leu-174, which is missing from the original *Pt*BSG sequence from Ensembl. The sequences were aligned using ClustalW software (Larkin *et al*., 2007).

The BSG orthologues were then tested against a panel of seven monoclonal antibodies that had been raised using a CHO cell-derived recombinant *Hs*BSG as the antigen (Koch *et al*., 1999). MEM-M6/6 is known to recognise an epitope on IgSF domain 2 of *Hs*BSG, and the others epitopes on domain 1 (Koch *et al*., 1999). The binding of these monoclonals to heat-treated *Hs*BSG was found to be significantly less than that to untreated *Hs*BSG, suggesting their epitopes are non-linear and heat-labile (Figure 35 B).

*Pt*BSG was recognised by all the monoclonals, apart from the anti-domain 2 antibody, MEM-M6/6 (Figure 35 C). *Gg*BSG showed clear binding to MEM-M6/6 and to the anti-domain 1 antibodies MEM-M6/1, MEM-M6/2 and MEM-M6/4. It did not appear to be recognised by MEM-M6/8 and MEM-M6/11 and showed reduced binding to MEM-M6/10. The recognition of *Pt*BSG and *Gg*BSG by monoclonals with non-linear epitopes, suggest that they are likely to have been expressed in their native conformation. The absence of binding of some of the monoclonals to *Pt*BSG and *Gg*BSG is probably due to non-conservation of their epitopes as a consequence of variations in the primary sequences of *Pt*BSG and *Gg*BSG relative to *Hs*BSG.

4.2.8 Differences in the binding of RH5 to the BSG orthologues were revealed by AVEXIS.

The BSG orthologues expressed as β-lactamase tagged pentameric 'preys' were tested against biotinylated *Pf*RH5 and *Pr*RH5 'baits' by AVEXIS to identify putative interactions (Figure 36). In addition to its known interaction with *Hs*BSG, *Pf*RH5 also showed some binding to *Pt*BSG (Figures 36 B and C). No interactions were observed between *Pf*RH5 and *Gg*BSG or between *Pr*RH5 and any BSG orthologue.

As a test for binding specificity, a 2-fold dilution series each of *Hs*BSG and *Pt*BSG, was subsequently tested against *Pf*RH5. A significant difference was observed in the binding
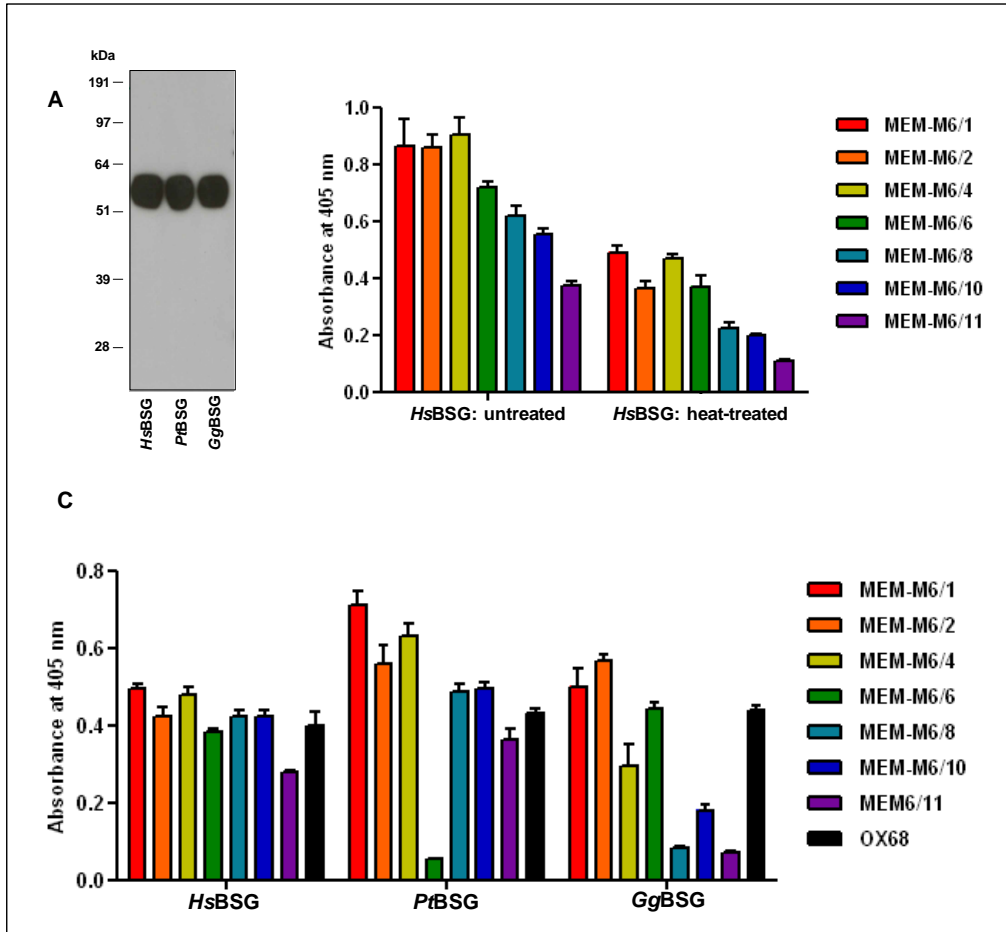
Figure 35. BSG orthologues from three primate species were recombinantly expressed and immunologically characterised. *Hs*BSG, *Pt*BSG and *Gg*BSG were expressed in the soluble form with C-terminal CD4 and biotin tags. These were then tested against a panel of seven mouse monoclonals raised against a *Hs*BSG antigen (Koch *et al*., 1999). **A)** A Western blot of the BSG orthologues performed using HRP-conjugated extravidin as the probe. The expected molecular weight of an un-glycosylated monomer of BSG is ~44 kDa. **B)** The panel of anti-BSG monoclonals were probed against untreated and heat-treated *Hs*BSG to identify the conformational properties of their epitopes (i.e. folded or linear). **C)** Recognition of the BSG orthologues by the anti-BSG monoclonals. OX68 was used as a positive control. Binding of the monoclonals to BSG was detected by ELISA. All ELISAs were performed on streptavidin-coated plates, using an alkaline phosphatase-conjugated anti-mouse antibody as the secondary. The graphically presented data indicate mean ± standard deviation; *n*=3.
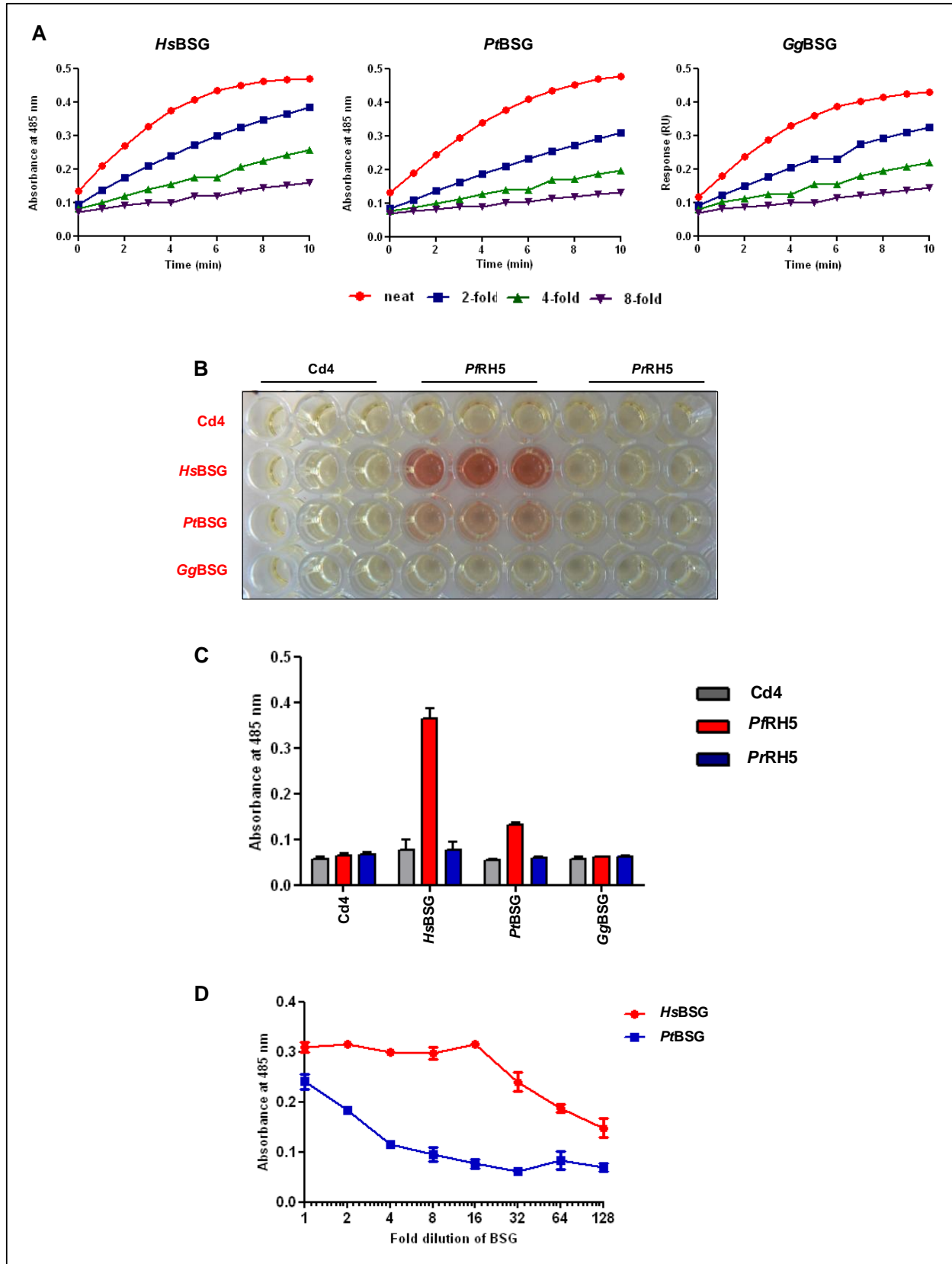
Figure 36. The interactions between recombinantly-expressed RH5 and BSG orthologues were analysed by AVEXIS. The BSG orthologues, expressed as β-lactamase tagged pentameric 'preys' were probed against biotinylated RH5 'baits' immobilised on streptavidin-coated plates. **A)** The BSG orthologues were normalised against each other by monitoring the turnover of nitrocefin in a time-course assay. **B)** and **C)** Results from the AVEXIS screen, in which each BSG 'prey' was tested against both *Pf*RH5 and *Pr*RH5. Cd4 in both 'bait' and 'prey' forms was used as the negative control. **D)** Binding of a 2-fold dilution series each of only *Hs*BSG and *Pt*BSG to *Pf*RH5, as tested by AVEXIS. The pentameric preys were incubated with the baits for 2 h in the AVEXIS assays and binding was detected by measuring nitrocefin turnover, 3 h after addition of the substrate. All steps were carried out at room temperature. The data in **C** and **D** are shown as mean ± standard deviation; *n*=3.

responses of *Hs*BSG and *Pt*BSG with *Pf*RH5, which is indicative of the *Pt*BSG-*Pf*RH5 interaction being of a substantially lower affinity than the *Hs*BSG-*Pf*RH5 interaction (Figure 36 D).

4.2.9 Affinity measurements for the RH5-BSG interactions were obtained by SPR.

SPR is a method of very high sensitivity which could be expected to reveal even interactions that are of too low affinity to be detected by AVEXIS. Therefore, the binding of BSG orthologues to *Pf*RH5 and *Pr*RH5 was also tested in reciprocal orientations by SPR, to identify any putative interactions that may have been missed in the previous AVEXIS screen.

For testing against biotinylated RH5 immobilised on a streptavidin-coated SPR sensor chip, the BSG orthologues were expressed with C-terminal Cd4 and hexa-His tags. After purification from the culture supernatant by affinity chromatography, the proteins were identified to be expressed at the correct size by SDS-PAGE (Figure 37 A). Glycosylation of the proteins was confirmed by staining the gel using a carbohydrate-specific periodic acid-Schiff reagent method. The proteins were subjected to gel filtration immediately prior to use in the SPR assays. Each BSG orthologue eluted from the gel filtration column as a single prominent peak with an elution volume (of ~ 35 ml) corresponding to a size of ~50 kDa, indicating a monomeric form (Figure 37 B). When tested against the RH5 orthologues both *Hs*BSG and *Pt*BSG showed binding to *Pf*RH5 (Figure 3 6C). The binding response observed was much lower in magnitude for *Pt*BSG in comparison with *Hs*BSG. No binding was observed with either *Gg*BSG or *Pr*RH5.

The SPR experiment was then repeated in the reverse orientation, with biotinylated BSG immobilised on the SPR chip and soluble RH5 injected across the sensor surfaces. As RH5 is a larger protein than BSG, performing the SPR experiment in this orientation was expected to
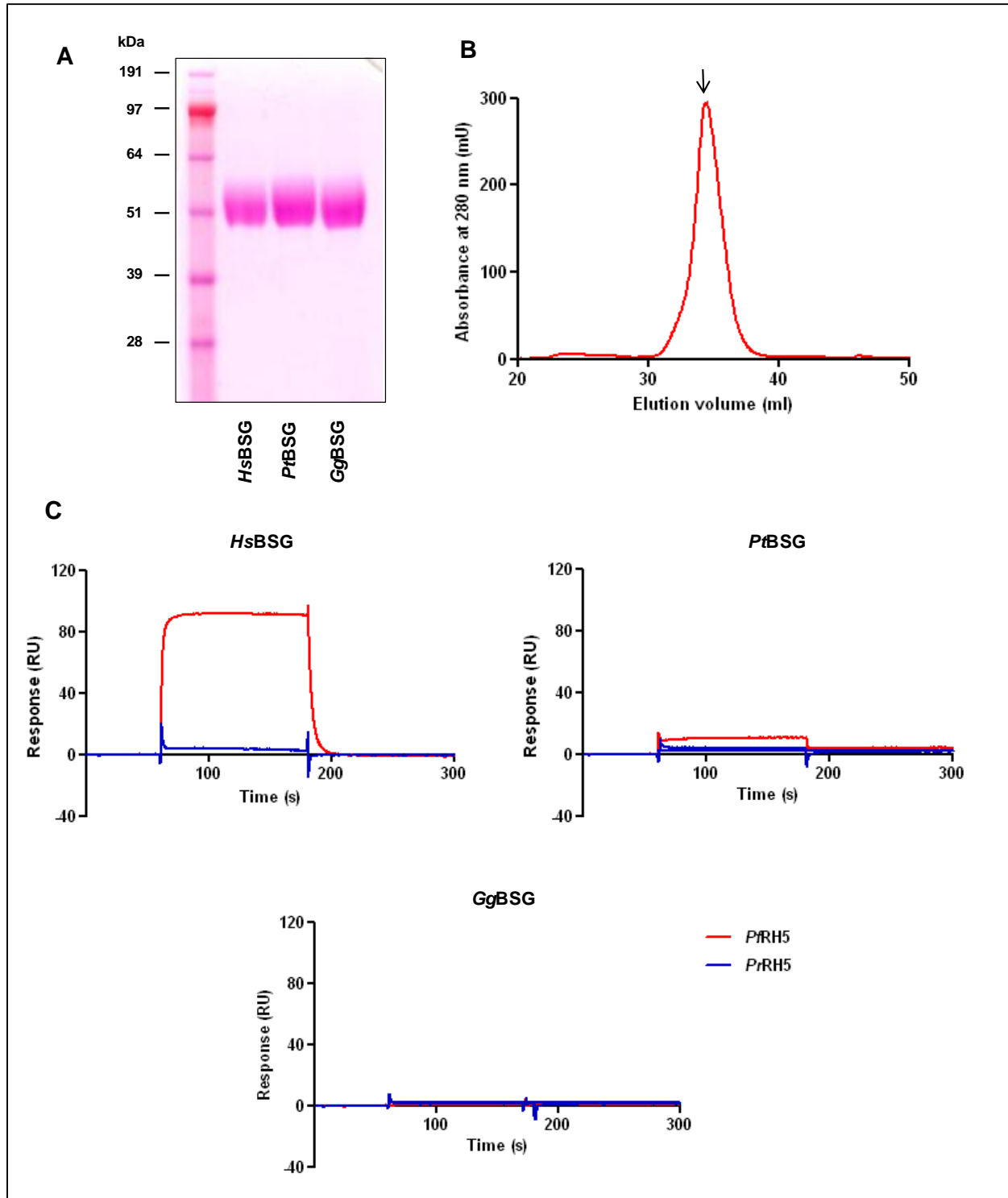
Figure 37. Recombinant hexa-His tagged BSG orthologues were purified from culture supernatants and tested against RH5 by SPR. A) Denaturing SDS-PAGE analysis of affinity-purified BSG orthologues. The proteins were visualised using a carbohydrate-specific dye to confirm glycosylation. **B)** The typical elution profile of a BSG orthologue from gel filtration. The peak fraction at ~35 ml is indicated by ↓. **C)** Reference subtracted sensorgrams from the injection of the BSG orthologues, each at 5 µM, over biotinylated *Pf*RH5 (red) and *Pr*RH5 (blue) immobilised on a streptavidin-coated sensor chip. The BSG proteins were injected at a flow rate of 20 μl/min, with a contact time of 120 s and a dissociation time of 200 s. The biotinylated baits were immobilised at Cd4 (reference)- 226 RU, *Pf*RH5-927 RU and *Pr*RH5-896 RU.

yield an improved signal to noise ratio with respect to the binding responses. For this experiment both *Pf*RH5 and *Pr*RH5 were expressed with C-terminal Cd4 and hexa-His tags. After purification from the culture supernatant by affinity chromatography on nickel-charged Sepharose, the proteins were analysed by SDS-PAGE under reducing conditions. Both proteins appeared to be expressed at the expected size of ~84 kDa (Figure 38 A). A significant proportion of each protein was however processed, generating fragments of ~64 kDa and ~28 kDa. When subjected to gel filtration, both *Pf*RH5 and *Pr*RH5 eluted in three peaks (Figure 38 B). The expected elution volume of the monomeric full-length forms of *Pf*RH5 (83.5 kDa) and *Pr*RH5 (84.4 kDa) was 32.8 ml. From the observed elution volumes of the peaks; 32.0 ml (peak 1), 35.3 ml (peak 2) and 38.0 ml (peak 3) in the case of *Pf*RH5 and 29.5 ml (peak 1), 34.2 ml (peak 2) and 38.9 ml (peak 3) for *Pr*RH5, the molecular weights of the species they contain were calculated to be ~100 kDa (peak 1), ~50 kDa (peak 2) and ~25 kDa (peak 3), indicating that they probably contain the ~84 kDa, ~64 kDa and ~28 kDa forms RH5 respectively. In the case of both *Pf*RH5 and *Pr*RH5 only the peak 2 fraction was used in the SPR binding studies with BSG.

In agreement with the observations from the previous AVEXIS and SPR experiments, no binding was observed with either *Pr*RH5 or *Gg*BSG (Figure 38 C). *Pf*RH5 showed much higher binding to *Hs*BSG than to *Pt*BSG.

To derive kinetic parameters for its interaction with *Hs*BSG and *Pt*BSG, a 2- fold dilution series of *Pf*RH5 was injected across the sensor surfaces (Figure 38 D). The k_a and k_d values estimated by globally fitting the reference subtracted sensorgrams to a 1:1 binding model (Figure 39 A) were consistent with previous data for the *Hs*BSG-*Pf*RH5 interaction (Crosnier *et al*., 2011) (Figure 39 B). The K_D values deduced from this analysis for the binding of *Pf*RH5 to *Hs*BSG and
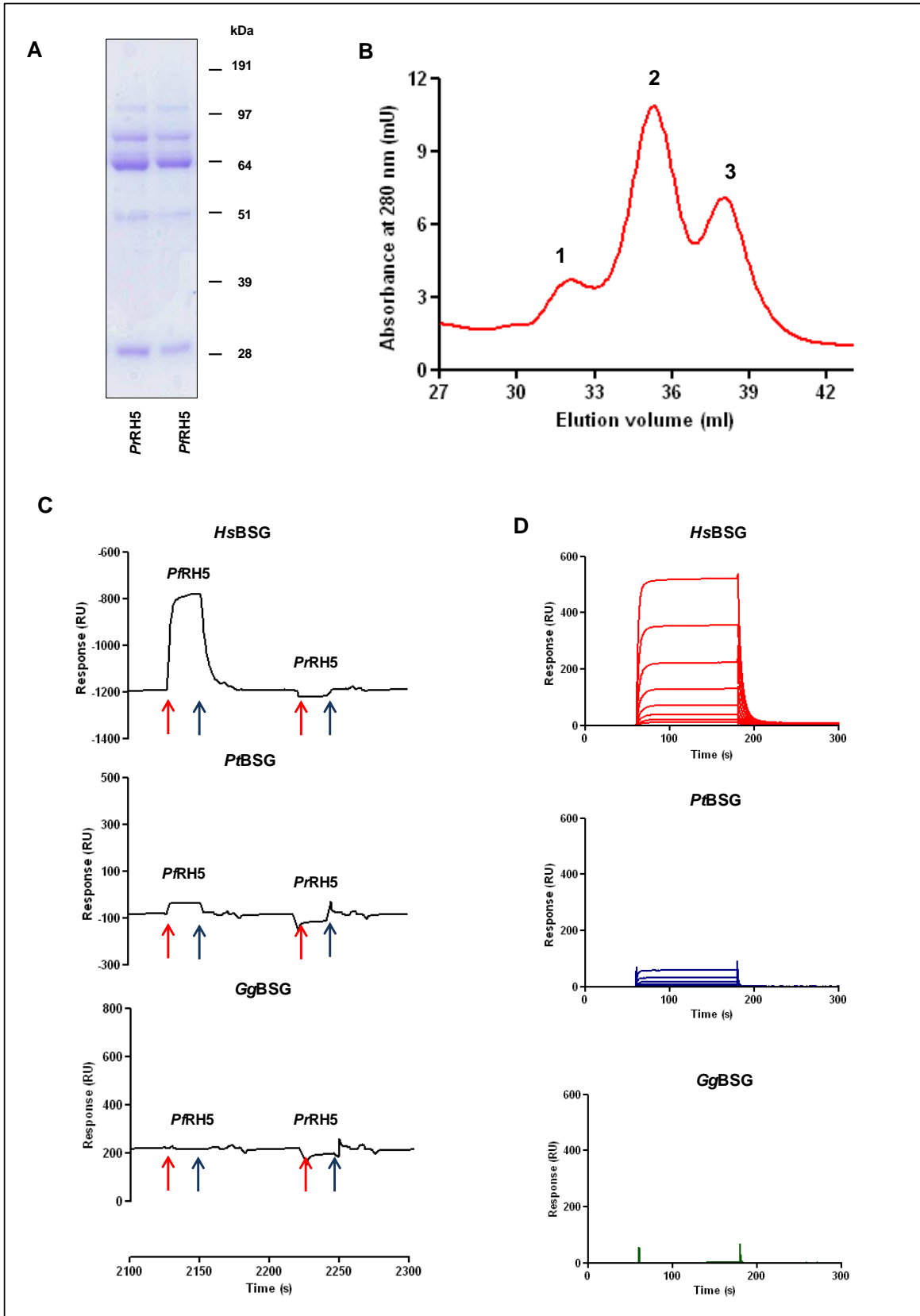
Figure 38. Hexa-His tagged RH5 orthologues were purified from culture supernatants and tested against BSG by SPR. A) Denaturing SDS-PAGE analysis of affinity-purified RH5 orthologues. The proteins were visualised using Coomassie brilliant blue. **B)** The typical elution profile of an RH5 orthologue from gel filtration. The three peak fractions, corresponding to the ~84 kDa (peak 1), ~64 kDa (peak 2) and ~28 kDa (peak 3) forms of RH5 are indicated. Only the peak 2 fractions of *Pf*RH5 and *Pr*RH5 were used in the SPR assays with BSG. **C)** Reference subtracted sensorgrams from the sequential injection of the RH5 orthologues, each at ~ 1 µM, over biotinylated *Hs*BSG, *Pt*BSG and *Gg*BSG immobilised on a streptavidin-coated sensor chip. The red and blue arrows represent the start and end of each injection. The RH5 proteins were injected at a flow rate of 30 µl/min for 30 s each. **D)** Reference subtracted sensorgrams from the injection of a 2-fold dilution series (0.02-1.1 µM) of *Pf*RH5, over the immobilised BSG orthologues. The RH5 proteins were injected at a flow rate of 20 µl/min, with a contact time of 120 s and a dissociation time of 200 s. The biotinylated baits were immobilised at Cd4 (reference) - 483 RU, *Hs*BSG, *Pt*BSG and *Gg*BSG- ~1050 RU.
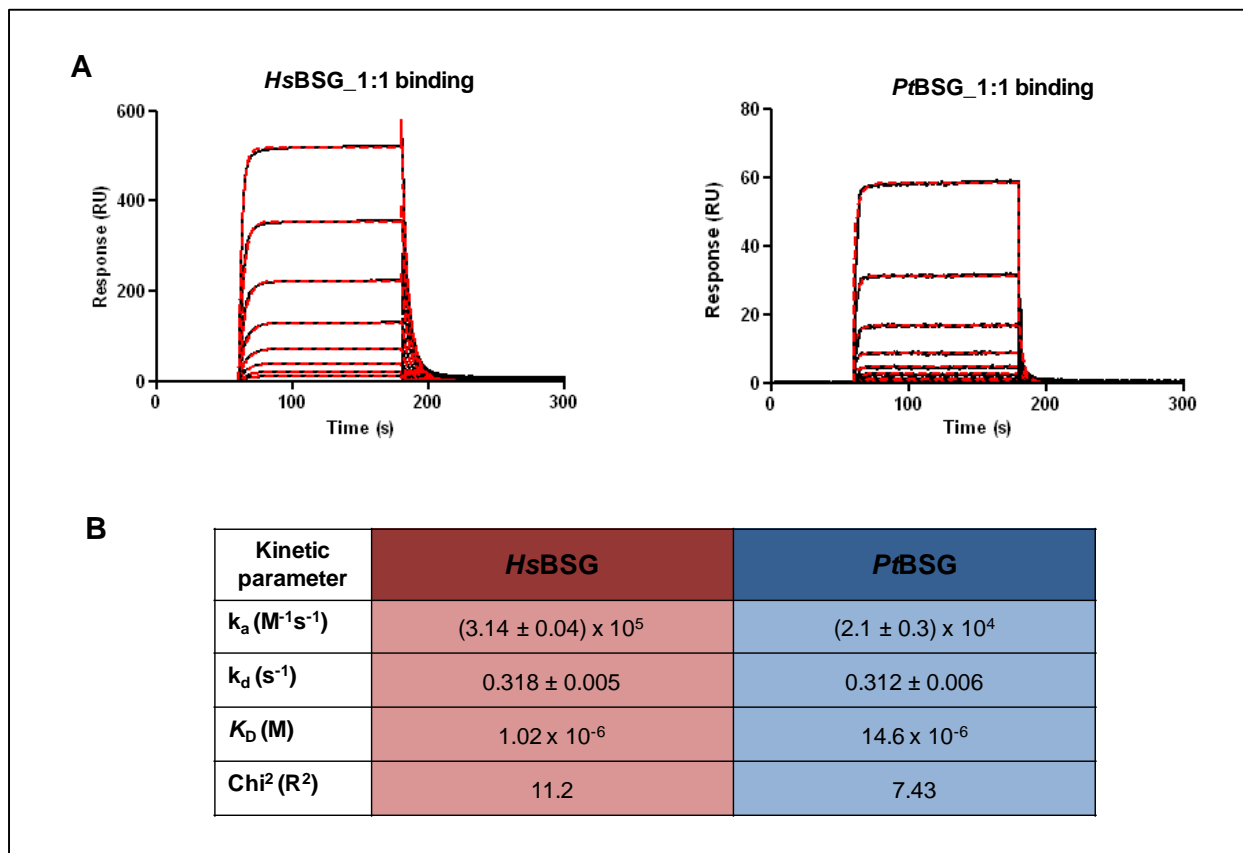
A

*Hs*BSG_1:1 binding

*Pt*BSG_1:1 binding

B

Kinetic parameter	*Hs*BSG	*Pt*BSG
k_a (M^{-1}s^{-1})	(3.14 ± 0.04) x 10^5	(2.1 ± 0.3) x 10^4
k_d (s^{-1})	0.318 ± 0.005	0.312 ± 0.006
K_D (M)	1.02 x 10^{-6}	14.6 x 10^{-6}
Chi^2 (R^2)	11.2	7.43

Figure 39. Equilibrium and kinetic parameters for the interactions of *Pf*RH5 with *Hs*BSG and *Pt*BSG were derived from the SPR data. A) Global fitting of the reference subtracted SPR sensorgrams from the binding of *Pf*RH5 to *Hs*BSG and *Pt*BSG, to a simple 1:1 binding model to derive kinetic parameters. The black lines represent experimental data and the red dotted lines, the fitted curves. **B)** Table with kinetic parameters estimated for the *Hs*BSG-*Pf*RH5 and *Pt*BSG-*Pf*RH5 interactions using the 1:1 model. The estimated values for the k_a, k_d and K_D are indicated with the standard errors.

*Pt*BSG were ~1.1 µM and ~14.6 µM respectively, suggesting an approximate 15-fold difference in affinity between the two interactions.

4.2.10 Site-directed mutants of human and chimpanzee BSG proteins were generated and tested for correct folding.

To identify BSG residues important for the observed host-specificity of the *Pf*RH5-BSG interaction, site-directed mutants of *Hs*BSG and *Pt*BSG were generated.

*Pt*BSG and *Hs*BSG are identical in domain 1, therefore, the reduced affinity of *Pt*BSG for *Pf*RH5 was hypothesised to be due to differences in domain 2. The nine residues in domain 2 of *Pt*BSG which are different from *Hs*BSG were mutated to the corresponding *Hs*BSG residues (Table 5). Additionally five residues in *Hs*BSG were mutated to those found in *Gg*BSG at the equivalent positions. Four of these residues are located in domain 1 and the fifth in domain 2. A Histidine residue was also inserted into the *Hs*BSG sequence at position 103, as found in *Gg*BSG (Table 5). The 15 site-directed *Pt*BSG (C1-C9) and *Hs*BSG (H1-H6) mutants, expressed with C-terminal CD4 and biotin tags, were normalised against each other and characterised by testing against the panel of seven anti-BSG monoclonals (Figure 40 A). All *Pt*BSG mutants were recognised by the anti-domain 1 monoclonals, as expected given that *Hs*BSG and *Pt*BSG are identical in domain 1. The anti-domain 2 monoclonal, MEM-M6/6, which doesn't bind *Pt*BSG, was observed to recognise one of the *Pt*BSG mutants, C8, suggesting that the MEM-M6/6 epitope, which was absent in *Pt*BSG, has been restored by a single residue change in this mutant. C8 was mutated at residue 191 from the negatively charged glutamic acid (found in *Pt*BSG) to positively charged lysine (found in *Hs*BSG). This change is likely to be important as residue 191 lies in a surface-exposed β-turn region (Yu *et al*., 2008).

Site-directed mutant			Location
*Pt*BSG	**C1**	V123 M	**Domain 2**
	C2	G145 E	
	C3	L163 S	
	C4	P164 Q	
	C5	E168 K	
	C6	L184 R	
	C7	N188 T	
	C8	E191 K	
	C9	V197 I	
*Hs*BSG	**H1**	F27 L	**Domain 1**
	H2	D32 E	
	H3	K75 E	
	H4	Q100 K	
	H5	Insertion H at 103	
	H6	S112 L	**Domain 2**

Table 5. Site-directed mutants of *Pt*BSG and *Hs*BSG. Nine residues in the IgSF domain 2 of *Pt*BSG were substituted with the residues at the corresponding positions in *Hs*BSG. Five residues in *Hs*BSG were mutated to those in *Gg*BSG at the equivalent locations. A Histidine residue was also inserted in *Hs*BSG at position 103, as found in *Gg*BSG.

All the *Hs*BSG mutants, apart from H1, H2 and H3, showed binding to all anti-*Hs*BSG monoclonal antibodies. H2 showed no binding to two monoclonals, MEM-M6/8 and MEM-M6/10 and reduced binding to MEM-M6/4. These data are consistent with the conclusions from an epitope-mapping study performed by Koch *et al*. (1999) for the anti-*Hs*BSG monoclonals (Figure 40 B). In their study, Koch *et al*. identified that MEM-M6/8 and MEM-M6/10 bind the same epitope with MEM-M6/4 recognising a proximal/overlapping epitope. Therefore residue 32, which was mutated in H2, is probably located within the MEM-M6/8+ MEM-M6/10 epitope. Both H1 and H3 showed reduced binding to MEM-M6/11. In the epitope-mapping study mentioned above, the epitope recognised by MEM-M6/11 had been identified to be a central one close to/overlapping with MEM-M6/1, MEM-M6/4 and MEM-M6/8 epitopes (Koch *et al*., 1999).

4.2.11 The affinities of BSG mutants for *P. falciparum* RH5 were compared to those of human and chimpanzee BSG.

Based on these results, four of the BSG mutants, C8, H1, H2 and H3, were selected for testing against *Pf*RH5 by SPR.

C8 was selected on the basis of its 'gain' of MEM-M6/6 binding activity in comparison to *Pt*BSG. MEM-M6/6 has previously been shown to block the *Pf*RH5-*Hs*BSG interaction (Crosnier *et al*., 2011), suggesting that its epitope may be located either at or near the *Pf*RH5 interaction surface. The epitope recognised by MEM-M6/8 and MEM-M6/10 is thought to overlap with/be adjacent to the MEM-M6/6 epitope (Koch *et al*., 1999), H2 was therefore chosen due to its observed 'loss-of-activity', relative to *Hs*BSG, in binding MEM-M6/8 and MEM-M6/10. The invasion of human erythrocytes by *P. falciparum* is inhibited at least partially by
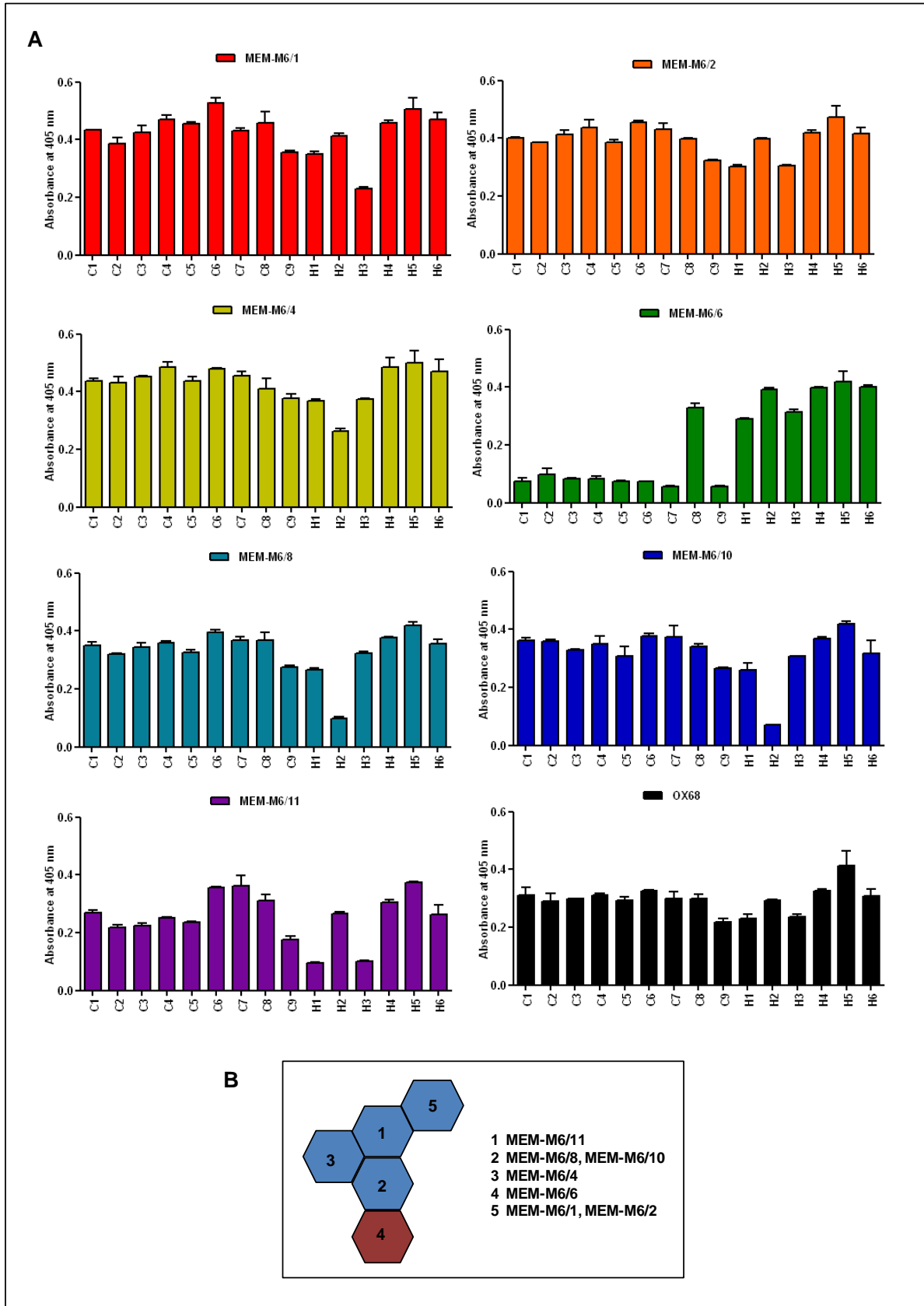
Figure 40. The site-directed mutants of *Pt*BSG and *Hs*BSG were immunologically characterised. A) The 15 site-directed mutants of *Hs*BSG and *Pt*BSG, expressed with C-terminal Cd4 and biotin tags, were tested against the panel of seven anti-*Hs*BSG mouse monoclonals by ELISA. OX68 was used as a positive control. The assays were performed on streptavidin-coated plates, using an alkaline phosphatase-conjugated anti-mouse antibody as the secondary. The data are shown as mean ± standard deviation; *n*=2. **B)** A schematic diagram indicating the relation of the epitopes recognised by the seven anti-*Hs*BSG monoclonals, as determined by Koch *et al*. (1999). Each hexagon represents one epitope. The epitopes with adjacent sides are recognised by antibodies which mutually inhibit each other's binding. Epitopes in IgSF domain 1 are shown in blue and that in domain 2 in red.

MEM-M6/1 and MEM-M6/4 (Cecile Crosnier and Zenon Zenonos, unpublished data). The MEM-M6/11 epitope is proposed to be adjacent to both the MEM-M6/1 and MEM-M6/4 epitopes. H1 and H3, which show reduced binding to MEM-M6/11, were hence also included as potential 'loss-of-function' mutants.

In the SPR screen, a 2-fold dilution series of purified *Pf*RH5 was injected across the biotinylated BSG mutants immobilised at equivalent amounts on streptavidin-coated sensor chips. *Hs*BSG and *Pt*BSG were included in the screen as controls (Figure 41 A). The reference subtracted sensorgrams were globally fitted to a 1:1 binding kinetic model to estimate values for the K_D. The K_D estimates for H2 and H3 were similar to that of *Hs*BSG, indicating no significant effect of these mutations on *Pf*RH5 binding. H1 exhibited a 7-fold lower affinity for *Pf*RH5 in comparison with *Hs*BSG, indicating a partial 'loss-of-function', suggesting that the F27L mutation in *Gg*BSG may play a critical role in restricting *Pf*RH5 binding. C8 on the other hand showed a significant 'gain-of-function' with a 4-fold higher affinity for *Pf*RH5 than even *Hs*BSG (Figure 41 B), confirming that the MEM-M6/6 binding site plays a key role in the *Pf*RH5-BSG interaction and suggesting that the K191E mutation in *Pt*BSG may play a key role in reducing affinity for *Pf*RH5.
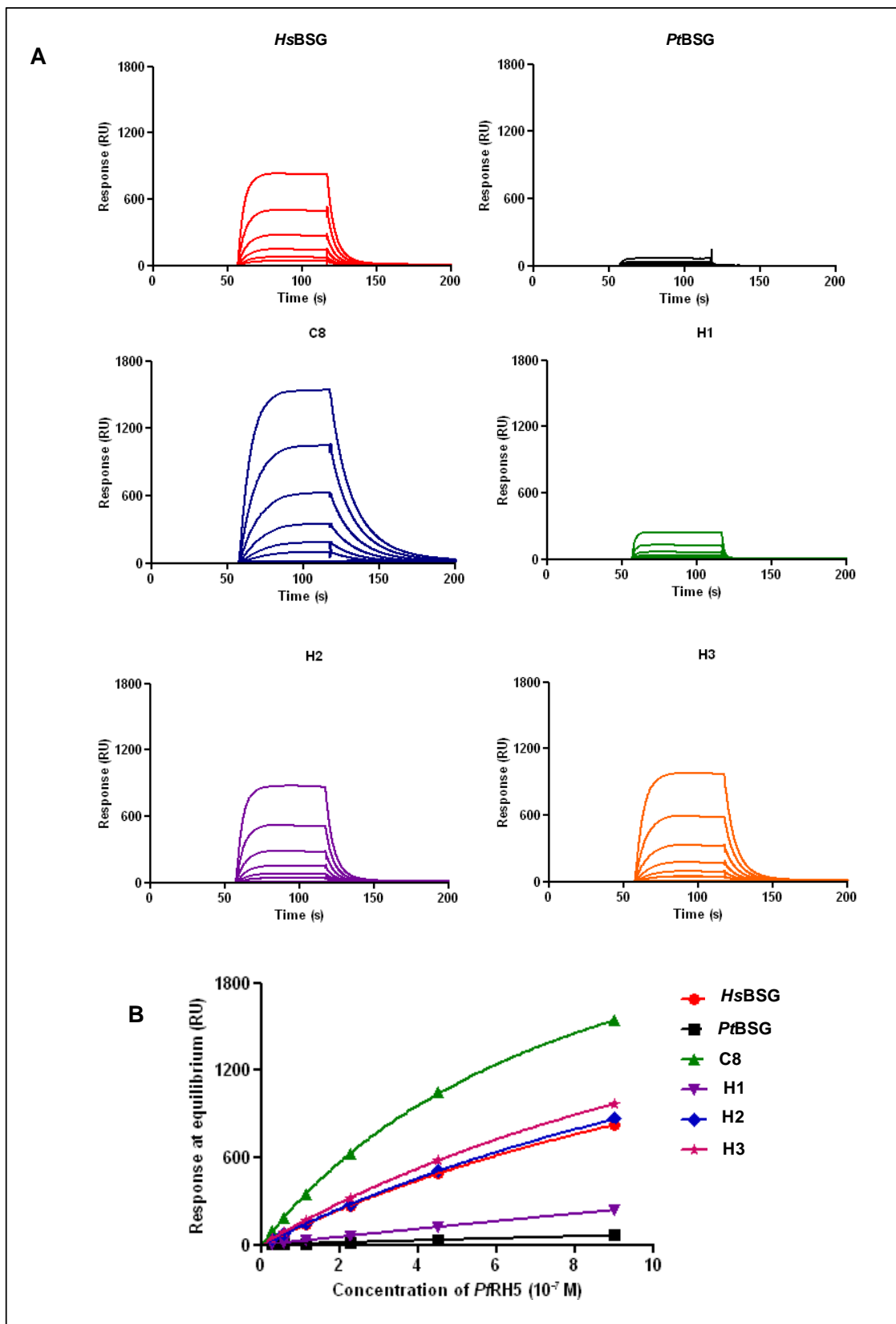
Figure 41. Four selected site-directed mutants of cBSG and hBSG were screened against *Pf*RH5, by SPR. The cBSG mutant, C8 and the hBSG mutants, H1, H2 and H3, were tested for binding to *Pf*RH5. The biotinylated BSG mutants were immobilised on streptavidin-coated SPR sensor chips at equivalent amounts and a 2-fold dilution series of purified *Pf*RH5 (0.03-0.9 µM) was injected over the sensor surfaces. Biotinylated hBSG and cBSG were included in the screen as controls. **A)** Reference subtracted sensorgrams from the binding of *Pf*RH5 to the BSG mutants. **B)** A chart showing the binding response at equilibrium *versus Pf*RH5 concentration for each of the BSG mutants. *Pf*RH5 was injected at a flow rate of 20 µl/min, with a contact time of 120 s and a dissociation time of 200 s. The biotinylated baits were immobilised at CHIP 1: Cd4 (reference) - 1362 RU, hBSG- 2774 RU, cBSG-2651 RU and C8-2652 RU; CHIP 2: Cd4 (reference)-1250 RU, H1-2576 RU, H2-2625 RU and H3-2662 RU.

4.3 DISCUSSION

Modern humans share a close evolutionary kinship with chimpanzees and gorillas, with the human-chimpanzee and human-chimpanzee-gorilla speciation events predicted to have occurred only around six and ten million years ago, respectively (Scally *et al*., 2012). These three species of primates share many anatomical and physiological features and have been found to be more than 95% identical in most known protein sequences. The closest relatives of the human malaria parasite, *P. falciparum* are also found within a family of chimpanzee and gorilla parasites, called *Laverania* and *P. falciparum* is even hypothesised to have adapted to humans after a zoonotic transfer event of a predecessor, *P. praefalciparum*, from gorilla (Liu *et al*., 2010; Rayner *et al*., 2011). Despite the genetic similarities between the *Laverania* parasites and among their hosts, in their natural environment, the different *Laverania* species have been observed to be strictly host-specific, with *P. reichenowi*, *P. billcollinsi* and *P. gaboni* restricted to chimpanzees and *P. praefalciparum*, *P. blacklocki* and *P. adleri* found only in gorillas (Liu *et al.*, 2010). The molecular basis of the *Laverania* host-specificity is poorly understood and its investigation is necessarily restricted by the lack of availability of the great ape parasite strains for laboratory-based testing. Chimpanzees and gorillas are also endangered species, so their use as *in vivo* models for experimentation is not ethically acceptable (Rayner *et al*., 2011). In this study, these limitations were overcome by the expression of parasite and great ape proteins recombinantly, thus, enabling interactions between them to be studied directly using *in vitro* biochemical methods.

The potential factors that contribute to the determination of host-specificity in the *Laverania* family may act at the vector/host or parasite/host interfaces. The scope of this study was limited to investigating the possible determinants of host-restriction at the stage of erythrocyte invasion

by the parasite. The process of erythrocyte entry by *Plasmodium* is mediated by interactions between surface proteins on the host and parasite cells (Chapter 1, Section 1.5). *P. falciparum*, the best characterised member of the *Laverania* family, is known to invade erythrocytes using multiple, partially redundant interactions between a broad repertoire of parasite ligands and erythrocyte receptors (Chapter 1, Sections 1.5 and 1.7). The EBL and RH families of parasite invasion ligands are loosely conserved across primate *Plasmodium* species and are known to be important for erythrocyte entry (Miller *et al*., 2002). From the known EBL and RH ligands, two proteins in particular, EBA175 and RH5, have gained attention as central players in erythrocyte invasion by *P. falciparum*. The interaction of RH5 with its erythrocyte receptor, BSG, is essential for invasion (Crosnier *et al*., 2011). The binding of EBA175 to its receptor, Glycophorin A, whilst not essential, is the primary ligand-receptor pair of its type used by many *P. falciparum* strains and invasion in the absence of EBA175 has been shown to almost always occur with lower efficiency (Narum *et al.*, 2000; Duraisingh *et al*., 2003). Both the EBA175-Glycophorin A and RH5-BSG interactions were investigated in this study for their potential contribution towards determining the differential host-species selectivity observed between members of the *Laverania* family.

4.3.1 The EBA175-Glycophorin A interaction may not contribute significantly to the establishment of host-species selectivity in *Laverania*.

The ability of EBA175 RII orthologues from the human parasite, *P. falciparum* and two chimpanzee parasites, *P. reichenowi* and *P. billcollinsi*, to recognise human erythrocytes and purified native human Glycophorin A, was probed using a number of complementary biochemical methods in this study. Native human Glycophorin A rather than recombinant Glycophorin A was used in this study, as the latter had been observed to be non-functional

(Chapter 3, Sections 3.2.5 and 3.2.6). The three EBA175 RII orthologues, produced in soluble recombinant form and multimerised by direct immobilisation on fluorescent beads, showed trypsin and neuraminidase-sensitive, but chymotrypsin-resistant association with human erythrocytes (Section 4.2,2, Figure 28). These properties are in agreement with the sialic-acid dependent recognition of Glycophorin A (a trypsin-sensitive, but chymotrypsin-resistant receptor) on the erythrocyte surface, by these orthologues (Camus and Hadley, 1985). However, to confirm binding of these orthologues to human Glycophorin A, their recognition of native Glycophorin A, extracted from human erythrocytes, was tested directly using an ELISA-based approach (Section 4.2.3). This assay revealed preferential binding of the EBA175 RII orthologues to sialylated human Glycophorin A over its asialylated derivative (Figure 29 C). The magnitude of the binding responses observed with *Pr*EBA175 RII and *Pb*EBA175 RII were somewhat lower in comparison to *Pf*EBA175 RII. Whilst this was suggestive of a lower affinity of the chimpanzee parasite proteins for human Glycophorin A, it could also have been due to the unpurified culture supernatants used for this assay containing different levels of functional EBA175. To circumvent this confounding factor, SPR was used to probe these interactions further. Prior to the SPR experiment, the EBA175 RII orthologues, purified from the culture supernatant by affinity chromatography, were subjected to gel filtration. The elution profiles were suggestive of the proteins being primarily monomeric (Figure 30 B). When the EBA175 RII orthologues were tested against native sialylated Glycophorin A, immobilised on a SPR sensor chip, a difference in the magnitude of the binding response was yet again observed between *Pf*EBA175 RII and *Pr*/*Pb*EBA175 RII (Figure 30 C). Equilibrium analysis of the reference-subtracted sensorgrams revealed an approximately 2-fold lower affinity of *Pr*/*Pb*EBA175 RII for human Glycophorin A, relative to *Pf*EBA175 RII (Section 4.2.4). Based

on previous studies, this ~2-fold lower affinity of *Pr/Pb*EBA175 RII for human Glycophorin A, could be attributed to a lower preference for the Neu5Ac found on the human protein (Section 4.1.2). The scale of the difference in *Pr/Pf*EBA175RII binding to human Glycophorin A was found to be much greater in previous studies, but this is likely due to differences in the assays being used, with the SPR assay used here giving a much greater range and sensitivity than previous cell-based assays (Martin *et al.*, 2005).

By co-crystallisation of *Pf*EBA175 RII with the substrate analogue, α-2,3-sialyllactose (containing Neu5Ac (α-2,3) Gal, essential for the recognition of human Glycophorin A by *Pf*EBA175), Tolia *et al.* (1995) identified the amino acid residues that were in contact with glycans at six potential binding sites (Chapter 3, Section 3.1.1). Comparison of 17 such 'glycan-binding' residues between *P. falciparum*, *P. reichenowi* and *P. billcollinsi* EBA175 RII sequences, revealed that 10 are conserved in all three species (Table 6). From the remaining seven, three each were conserved only either between *Pf*EBA175 RII and *Pr*EBA175 RII or between *Pf*EBA175RII and *Pb*EBA175 RII. Only one residue, located at position 697, was observed to be divergent in both *Pr*EBA175 RII and *Pb*EBA175 RII from *Pf*EBA175 RII. Overall, ~76% of the 'glycan-binding' residues found in *Pf*EBA175 RII were conserved in *Pr*/*Pb*EBA175 RII. This relatively high conservation of 'glycan-binding' residues may account for the fairly low difference in affinity observed between *Pf*EBA175 RII and *Pr*/*Pb*EBA175 RII, for Neu5Ac-carrying human Glycophorin A.

Glycan	Residue number	*Pf*EBA175	*Pr*EBA175	*Pb*EBA175	DBL domain
1/2	583	K	K	R	F2
	586	D	D	D	F2
	172	K	K	K	F1
3/4	694	N	N	N	F2
	695	N	N	N	F2
	696	Y	N	Y	F2
	697	K	R	T	F2
	698	M	I	M	F2
	177	N	N	N	F1
5/6	484	T	T	T	F2
	485	K	K	K	F2
	486	D	D	V	F2
	487	V	V	I	F2
	559	Y	Y	Y	F2
	686	Q	I	Q	F2
	690	Y	Y	Y	F2
	173	N	N	N	F1

Table 6. The conservation of residues at six 'glycan-binding' sites between the EBA175 orthologues from *P. falciparum*, *P. reichenowi* and *P. billcollinsi*. 17 EBA175 residues identified by Tolia *et al.* (2005) as being in contact with glycans at six putative binding sites in the *Pf*EBA175RII+α-2,3-sialyllactose co-crystal structure were compared between the EBA 175 orthologues. Residues identical between all three orthologues are highlighted in dark pink. Residues identical only between *Pf*EBA175 and either *Pr*EBA175 or *Pb*EBA175 are highlighted in light pink.

4.3.2 The RH5-BSG interaction is likely to be a significant determinant of *Laverania* host-specificity.

The RH5 orthologues from *P. falciparum* and *P. reichenowi* were tested for species-specific interactions with human erythrocytes and with recombinantly-expressed BSG orthologues from human, chimpanzee and gorilla, in this study. The *Pf*RH5 and *Pr*RH5 orthologues share approximately 68% sequence identity (Figure 31), however, *Pr*RH5 was not recognised by any of 26 mouse monoclonal antibodies binding to *Pf*RH5 (Figure 32 C). Even a rabbit polyclonal raised against *Pf*RH5 exhibited only barely detectable binding to *Pr*RH5 (Figure 32 D). This data suggests that immunogenic, surface-exposed regions may not be well conserved between *Pf*RH5 and *Pr*RH5. Similar, neuraminidase-insensitive, low-level binding to human erythrocytes was observed with both *Pf*RH5 and *Pr*RH5 (Figures 33 A and B). The interaction of *Pf*RH5 with *Hs*BSG is known to be sialic-acid independent, moreover, the level of expression of BSG on the surface of human erythrocytes is relatively low (in comparison to Glycophorin A, Figures 33 C and D). Therefore, the properties of the observed interactions of *Pf*RH5 and *Pr*RH5 with human erythrocytes are consistent with the recognition of BSG on the erythrocyte surface. However, *Pr*RH5 showed no detectable binding to *Hs*BSG, *Pt*BSG or *Gg*BSG when tested directly against these recombinant proteins, both by AVEXIS and by SPR (Figures 36, 37 and 38). One possible explanation for the observed behaviour of *Pr*RH5 is its recognition of a receptor other than BSG on the chimpanzee erythrocyte surface. The observation by Hayton *et al*. (2008) of 28 kDa fragments of *Pf*RH5 proteins carrying different polymorphisms recognising different erythrocyte proteins, supports this theory of a possible 'receptor-switch', between hosts.

In this study, *Pf*RH5 was observed to bind to *Pt*BSG with an affinity 15-fold lower than that for *Hs*BSG and no interaction could be detected between *Pf*RH5 and *Gg*BSG (Figures 37, 37, 38

and 39), suggesting clear host-species selectivity in receptor recognition. To identify residues that confer this specificity, site-directed mutants of *Pt*BSG and *Hs*BSG were generated and a selection of these was tested against *Pf*RH5 in a preliminary screen (Table 6 and Figure 41). Both IgSF domains 1 and 2 of *Hs*BSG have been implicated in *Pf*RH5 binding (Crosnier *et al*., 2011). *Pt*BSG is different from *Hs*BSG only in nine residues, all located in domain 2 (Figure 34). Possible 'gain-of-function' *Pt*BSG mutants were made by replacing these divergent residues with the corresponding *Hs*BSG residues (Table 5). *Hs*BSG is different from *Gg*BSG in both domains 1 and 2 and potential 'loss-of-function' *Hs*BSG mutants were produced by replacing six variant residues (five located in domain 1 and one in domain 2) with those found in *Gg*BSG at the equivalent positions (Figure 34 and Table 5).

*Pt*BSG was not recognised by the anti-hBSG monoclonal MEM-M6/6 (Figure 35). This monoclonal has previously been shown to inhibit the interaction between *Hs*BSG and *Pf*RH5, suggesting that its epitope is likely to be located either at/near the *Pf*RH5 binding site on *Hs*BSG (Crosnier *et al*., 2011). The MEM-M6/6 epitope was however observed to have been 'recovered' in one of the *Pt*BSG mutants, C8 (E191K) and testing this mutant by SPR revealed complete restoration of *Pf*RH5 binding (Figures 40 and 41). Indeed, the affinity of this mutant for *Pf*RH5 was even 4-fold higher than that of *Hs*BSG. The data therefore suggest that the single residue difference between *Hs*BSG and *Pt*BSG at position 191 is responsible for the much weaker binding of *Pf*RH5 by *Pt*BSG relative to *Hs*BSG. Residue 191 is located in an accessible β-turn region proximal to the IgSF domain 1 and a change at this position from a positively-charged amino acid (found in *Hs*BSG) to a negatively-charged one (found in *Pt*BSG) seems likely to have a significant influence (Yu *et al*., 2008 and Figure 42).

*Gg*BSG was not recognised by the anti-*Hs*BSG monoclonals, MEM-M6/8 and MEM-M6/11, and also showed reduced binding to MEM-M6/10 (Figure 35). The epitope recognised by MEM-M6/8 and MEM-M6/10 is predicted to overlap with/be adjacent to the MEM-M6/6 epitope, whereas the MEM-M6/11 epitope is postulated to be proximal to both MEM-M6/1 and MEM-M6/4 epitopes (Koch *et al*., 1999). In addition to MEM-M6/6, both MEM-M6/1 and MEM-M6/4 have been observed to block the *Pf*RH5-*Hs*BSG interaction at least partially and their epitopes are therefore also likely to be close to the *Pf*RH5 binding site on *Hs*BSG (Cecile Crosnier and Zenon Zenonos, unpublished data).

From the *Hs*BSG mutants, H2 (D32E) showed no binding to both MEM-M6/8 and MEM-M6/10, suggesting that residue D32 is part of the MEM-M6/8+ MEM-M6/10 epitope (Figure 40). H1 (F27L) and H3 (K75E) mutants showed reduced binding to MEM-M6/11, indicating a change in these mutants close to the *Pf*RH5-*Hs*BSG interaction surface (Figure 40). Analysis of the H1, H2 and H3 mutants by SPR revealed that H2 and H3 bind to *Pf*RH5 with almost the same affinity as *Hs*BSG, indicating no significant 'loss-of-function' (Figure 41). H1 however showed a 7-fold lower affinity for *Pf*RH5 than *Hs*BSG, indicating that the change at position 27 of the primary sequence from the aromatic residue tryptophan (found in *Hs*BSG) to the non-aromatic residue leucine (found in *Gg*BSG), is one likely contributing factor to the inability of *Gg*BSG to bind *Pf*RH5. In *Hs*BSG, F27 is solvent-exposed and located on a β-strand constituting IgSF domain 1 (Yu *et al*., 2008, Figure 42).

Overall, the data from the screen of BSG mutants suggests that the residues K191 and F27 of *Hs*BSG are important for the interaction with *Pf*RH5 and that the non-conservation of these residues in *Pt*BSG and *Gg*BSG respectively may be responsible (at least partially in the case of *Gg*BSG) for the observed host-specificity of *Pf*RH5 binding.

Residue E92, located on a β-turn region of domain 1, has previously been identified to be important for the binding of *Hs*BSG to *Pf*RH5 (Crosnier *et al*., 2011). The mutation E92K, responsible for the Ok^{a-} blood type, has been shown to decrease the affinity of *Hs*BSG for *Pf*RH5 by 2-fold (Crosnier *et al*., 2011). In the X-ray crystal structure of *Hs*BSG, K191 is located ~27 Å and ~37 Å from F27 and E92 respectively, whereas F27 and E92 are located ~16 Å apart across domain 1 (Yu *et al*., 2008). Protein-protein interaction surfaces are in general fairly large, with standard sizes ranging from ~1200-~2000 Å^2, therefore the three residues, K191, F27 and E92 are all likely to be accommodated in the *Pf*RH5 binding site of BSG (Moreira *et al*., 2007).

4.4 CONCLUSION

In this study, only a 2-fold difference in the affinity for human Glycophorin A was observed between the EBA175 RII orthologues from *P. falciparum*, *P. reichenowi* and *P. billcollinsi*, suggesting that the EBA175RII-Glycophorin A interaction may not be a significant determinant of the observed host-selectivity within the *Laverania* family, unlike previous suggestions (Martin *et al.*, 2005). *P. falciparum* RH5 on the other hand showed clear host-species specificity in its binding of Basigin orthologues from human, chimpanzee and gorilla. No binding of *P. falciparum* RH5 to gorilla BSG was observed and its binding to chimpanzee BSG was approximately 15-fold weaker than its interaction with human BSG. The binding of *P. falciparum* RH5 to human BSG is essential for the invasion of human erythrocytes by the parasite, therefore the relative differences in the interactions of *P. falciparum* RH5 with chimpanzee and gorilla Basigin, may account for the observed lack of *P. falciparum* infection in their wild-living populations. This study only investigated the contributions of two known parasite ligand-erythrocyte receptor interactions towards host-species selection amongst *Laverania* parasites. In order to gain a more complete understanding of how host selectivity of

Laverania is imposed at the stage of erythrocyte entry, the systematic approach used in this study should necessarily be extended to other known parasite ligand-host receptor interactions, such as RH4-CR1.
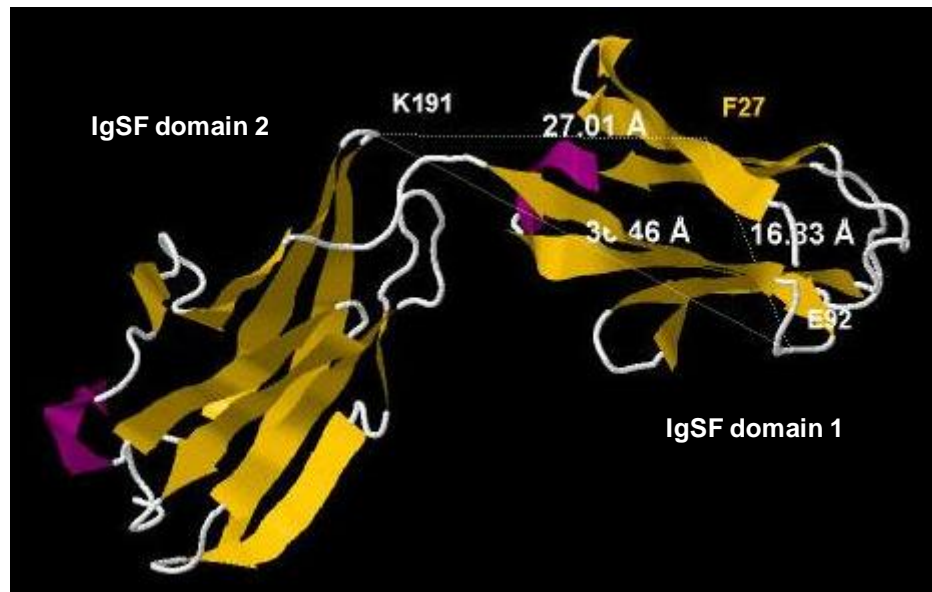
Figure 42. The structural organisation of the two IgSF domains of *Hs*BSG with the positions of the residues implicated in *Pf*RH5 binding, K191, F27 and E92 annotated. A schematic representation of the X-ray crystal structure of *Hs*BSG as determined by Yu *et al*. (2008) is shown (PDB ID: 3B5H). The residues predicted to be located at the *Pf*RH5 binding site are indicated with the approximate distances between them, K191-F27: 27.01 Å, K191-E92: 36.46 Å, F27-E92: 16.33 Å.

4.5 BIBLIOGRAPHY

Baum, J., Chen, L., Healer, J., Lopaticki, S., Boyle, M., Triglia, T., Ehlgen, F., *et al*. (2009). Reticulocyte-binding protein homologue 5 - an essential adhesin involved in invasion of human erythrocytes by *Plasmodium falciparum*. *International Journal for Parasitology*, *39*(3), 371-80.

Blacklock, B. & Adler, S. (1922) A parasite resembling *Plasmodium falciparum* in a chimpanzee. *Annals of Tropical Medicine and Parasitology*,*16*, 99-106.

Camus, D., & Hadley, T. J. (1985). A *Plasmodium falciparum* antigen that binds to host erythrocytes and merozoites. *Science*, *230*(4725), 553-556.

Crosnier, C., Bustamante, L. Y., Bartholdson, S. J., Bei, A. K., Theron, M., Uchikawa, M., Mboup, S., *et al*. (2011). Basigin is a receptor essential for erythrocyte invasion by *Plasmodium falciparum*. *Nature*, *480*(7378), 534-7.

Duraisingh, M. T., Maier, A. G., Triglia, T., & Cowman, A. F. (2003). Erythrocyte-binding antigen 175 mediates invasion in *Plasmodium falciparum* utilizing sialic acid-dependent and -independent pathways. *Proceedings of the National Academy of Sciences of the United States of America*, *100*(8), 4796-801.

Duval, L., Fourment, M., Nerrienet, E., Rousset, D., Sadeuh, S. A., Goodman, S. M., Andriaholinirina, N. V., *et al*. (2010). African apes as reservoirs of *Plasmodium falciparum* and the origin and diversification of the Laverania subgenus. *Proceedings of the National Academy of Sciences of the United States of America*, *107*(23), 10561-6.

Duval, L., & Ariey, F. (2012). Ape *Plasmodium* parasites as a source of human outbreaks. *Clinical Microbiology and Infection*, *18*(6), 528-32.

Flicek, P., Amode, M. R., Barrell, D., Bea,l K., Brent, S., Chen, Y., Clapham, P., *et al.* (2011). Ensembl 2011. *Nucleic Acid Research*,*39*, D800-6

Hayton, K., Gaur, D., Liu, A., Takahashi, J., Henschen, B., Singh, S., Lambert, L., *et al*. (2008). Erythrocyte binding protein PfRH5 polymorphisms determine species-specific pathways of *Plasmodium falciparum* invasion. *Cell Host & Microbe*, *4*(1), 40-51.

Koch, C., Staffler, G., Hüttinger, R., Hilgert, I., Prager, E., Cerný, J., Steinlein, P., *et al*. (1999). T cell activation-associated epitopes of CD147 in regulation of the T cell response, and their definition by antibody affinity and antigen density. *International Immunology*, *11*(5), 777-86.

Larkin, M. A., Blackshields, G., Brown, N. P., Chenna. R., McGettigan, P. A., McWilliam, H., *et al*. (2007) Clustal W and Clustal X version 2.0. *Bioinformatics*, *23*(21), 2947-8.

Liu, W., Li, Y., Learn, G., Rudicell, R., & Robertson, J. (2010). Origin of the human malaria parasite *Plasmodium falciparum* in gorillas. *Nature*, *467*(7314), 420-425.

Martin, M. J., Rayner, J. C., Gagneux, P., Barnwell, J. W., & Varki, A. (2005). Evolution of human-chimpanzee differences in malaria susceptibility: relationship to human genetic loss of N-glycolylneuraminic acid. *Proceedings of the National Academy of Sciences of the United States of America*, *102*(36), 12819-24.

Miller, L. H., Baruch, D. I., Marsh, K., & Doumbo, O. K. (2002). The pathogenic basis of malaria. *Nature*, *415*(6872), 673-9.

Moreira, I. S., Fernandes, P. A., & Ramos, M. J. (2007). Hot spots—A review of the protein–protein interface determinant amino-acid residues. *Proteins*, *68*(4), 803-12.

Muchmore, E. A., Diaz, S., & Varki, A. (1998). A structural difference between the cell surfaces of humans and the great apes. *American Journal of Physical Anthropology*, *107*(2), 187-98.

Narum, D. L., Haynes, J. D., Fuhrmann, S., Liang, H., Hoffman, S. L., Sim, B. K. L., Moch, K., *et al*. (2000). Antibodies against the *Plasmodium falciparum* receptor binding domain of EBA-175 block invasion pathways that do not involve sialic acids. *Infection and Immunity*, *68*(4), 1964-6.

Ozwara, H., Kocken, C. H., Conway, D. J., Mwenda, J. M., & Thomas, A. W. (2001). Comparative analysis of *Plasmodium reichenowi* and *P. falciparum* erythrocyte-binding proteins reveals selection to maintain polymorphism in the erythrocyte-binding region of EBA-175. *Molecular and Biochemical Parasitology*, *116*(1), 81-4.

Prugnolle, F., Ayala, F., Ollomo, B., Arnathau, C., Durand, P., & Renaud, F. (2011). *Plasmodium falciparum* is not as lonely as previously considered. *Virulence*, *2*(1), 71-76.

Rayner, J. C., Liu, W., Peeters, M., Sharp, P. M., & Hahn, B. H. (2011, May). A plethora of Plasmodium species in wild apes: a source of human infection? *Trends in Parasitology*,*27*(5), 222-9.

Scally, A., Dutheil, J. Y., Hillier, L. W., Jordan, G. E., Goodhead, I., Herrero, J., Hobolth, A., *et al*. (2012). Insights into hominid evolution from the gorilla genome sequence. *Nature*, *483*(7388), 169-175.

Sharp, P. M., Liu, W., Learn, G. H., Rayner, J. C., Peeters, M., & Hahn, B. H. (2011). Source of the human malaria parasite *Plasmodium falciparum. Proceedings of the National Academy of Sciences of the United States of America*, *108*(38), E744-5.

Sim, B. K. L., Narum, D. L., Chattopadhyay, R., Ahumada, A., Haynes, J. D., Fuhrmann, S. R., Wingard, J. N., *et al*. (2011). Delineation of stage specific expression of *Plasmodium falciparum* EBA-175 by biologically functional region II monoclonal antibodies. *PloS One*, *6*(4), e18393.

Yu, X. L., Hu, T., Du, J. M., Ding, J. P., Yang, X. M., Zhang, J., Yang, B., *et al*. (2008). Crystal structure of HAb18G/CD147: implications for immunoglobulin superfamily homophilic adhesion. *The Journal of Biological Chemistry*, *283*(26), 18,056-65.

Zdobnov, E. M., Apweiler, R. (2001). InterProScan--an integration platform for the signature-recognition methods in InterPro. *Bioinformatics*, *17*(9), 847-8.